J. Mech. Phys. Solids 192 (2024) 105790

Contents lists available at ScienceDirect

Journal of the Mechanics and Physics of Solids

journal homepage: www.elsevier.com/locate/jmps

Hyperinelasticity: An energy-based constitutive modelling approach to isothermal large inelastic deformation of polymers. Part I

Afshin Anssari-Benam

Cardiovascular Engineering Research Lab (CERL), School of Mechanical and Design Engineering, University of Portsmouth, Anglesea Road, Portsmouth, PO1 3DJ, United Kingdom

ARTICLE INFO

Keywords:
Inelasticity
Large deformations
Polymers
Unified model
Constitutive modelling
Softening

ABSTRACT

The foundation of a new concept, coined here as *hyperinelasticity*, is presented in this work for modelling the isothermal elastic and inelastic behaviours of polymers. This concept is based on the premise that both the elastic and inelastic behaviours of the subject specimen in the primary loading path may be characterised by a single constitutive law derived from a comprehensive deformation energy W, akin to hyperelasticity, whose constitutive parameters determine and capture both the elastic and inelastic behaviours without the need for additional flow/yield/damage parameters. This *core* hyperinelastic model captures the elastic and inelastic behaviours in the primary loading path. It is then further specialised, by augmenting the embedded constitutive parameters in the *core* model, for capturing the inelasticity of the unloading behaviour and the rate of deformation effects. The former is done by devising and incorporating a discontinuous inelasticity variable into the *core* function, and the latter is achieved by considering that the *core* model parameters can evolve with, i.e., be a function of, the deformation rate. Examples of the application of the *core* and *augmented* hyperinelastic models to a wide range of extant experimental datasets will be presented, ranging from foams, glassy and semi-crystalline polymers to hydrogels and liquid crystal elastomers. The loading modes encompass both tensile and compressive deformations. With a reduced set of number of model parameters (compared with the existing models in the literature), simplicity of implementation (as essentially a straightforward extension to hyperelasticity), and encouraging accuracy in the modelling results, the concept of *hyperinelasticity* together with the presented hyperinelastic model are proposed as a unified modelling means for capturing the elastic and inelastic behaviours of polymers.

1. Introduction

A concurrent topic of interest in the literature concerning the finite deformation of polymers is to find a model, i.e., a constitutive law, for the theoretical treatment of the experimentally observed mechanical behaviour of the subject specimen, over the whole range of deformation. Two major challenges preside over this endeavour, encapsulated within the foregoing statement. First, the whole range of deformation includes both what is referred to as *elastic* and *inelastic* features of deformation — specific features of note will be cast definitively in the sequel. Second, the subject specimen can be of generic type, ranging from (multi-network) hydrogels, foams, glassy and/or semi-crystalline polymers to liquid crystal elastomers (LCEs) etc. The literature is yet to introduce

E-mail address: afshin.anssari-benam@port.ac.uk.

https://doi.org/10.1016/j.jmps.2024.105790
Received 1 June 2024; Received in revised form 27 June 2024; Accepted 18 July 2024
Available online 22 July 2024

a unified, general, versatile model for accurately capturing those 'elastic' and 'inelastic' features, applicable across various polymer types. Suggesting one such model is at the crux of this manuscript.

The elastic and inelastic features of interest under large deformations in various polymers, while having similar traits, have nuanced differences. Those traits in general include some or all of the following[1]: (a) an initial linear or nonlinear elastic behaviour; (b) a nonlinear behaviour leading up to a peak stress; (c) a drop in the stress often proceeded by a plateau; and (d) a hardening phase leading to the fracture/failure. Polymeric foams, for example, under compression exhibit an (almost) linear elastic initial region, followed by an inelastic behaviour which includes a drop in the stress and/or plateau, and a final 'densification' phase leading to a hardening behaviour. No such distinct sequential behaviour is observed under tension. See the recent work of Lee et al. (2020) for a more detailed description of these phases in relation to polyurethane and polystyrene foams. Glassy polymers, on the other hand, show a nonlinear behaviour in the elastic range up to a peak (initial yield) stress under tensile deformation, accompanied by the inelastic phase which encompasses stress softening and a drop in the stress, and a hardening behaviour at larger strains. A qualitative description of this behaviour may be found in Boyce et al. (1988), and specific stress–deformation curves in relation to epoxy specimens have been reported by Uchida et al. (2022). Semi-crystalline polymers show a rapid initial stiffening behaviour in their elastic response — thought to be typically of up to 10% strains (van Dommelen et al., 2003), proceeded by significant nonlinearity leading to plateauing of stress (which is considered to signify yield), and again a hardening behaviour at larger levels of deformation. See also (Ayoub et al., 2010) for exemplar stress–deformation curves. Multi-network hydrogels demonstrate a similar behaviour under tensile deformation; however, the amplitude of drop in stress is lower in comparison with glassy and semi-crystalline polymers, and the proceeding plateau in their stress–deformation curves are much more pronounced than those in the aforementioned polymers. See, e.g., Vernerey et al. (2018) for quantitative examples using quadruple-network hydrogel specimens. Last but not least, the phenomenon of 'soft elasticity' in LCEs, while not an inelastic feature, is an elastic behaviour which leads to the loss of convexity (Lee and Bhattacharya, 2023; Lee et al., 2023), and may reflect itself as either a plateau (e.g., Rezaei et al., 2024) or a peak-and-trough (e.g., Martin Linares et al., 2020) in the stress–deformation curve, distinct from the stress drop or softening behaviours described in the preceding examples for other polymers.

The discernible characteristic, and nature, of these *elastic* and *inelastic* behaviours in various elastomers, as recounted in the foregoing, are such that no unified model has yet been shown capable of application to these variety of polymers and behaviours. From the early attempts in the theoretical treatment of the observed inelasticity in stress–strain curves of polymers by Haward and Thackray (1968), which considered three sequences of linear elastic, yield and hardening behaviours, to the more recent models inspired by that work such as those by Boyce et al. (1988), Ahzi et al. (2003), Ayoub et al. (2010) and Uchida et al. (2022) *inter alia*, the proposed models may best be applied only to certain polymer types and behaviours, and suffer from the common drawbacks of inaccurate predictions of the nonlinear behaviours, overshooting the peak stress and/or mis-predicting the plateau etc. The models by Anand and Ames (2006) and Anand et al. (2009) provide an improvement to those modelling results; however, at the cost of an excessive number of model parameters which may render an objective identification and interpretation of the parameter values challenging. Adding parameters to the main constitutive law to act as a switch so that certain attributes are activated/deactivated when the strain or stress reaches a certain value (e.g., Lee et al. (2020) for the stress drop/softening), while helps emulating the macroscopic behaviour, introduces non-smoothness problems in that an exact value at which the roll-over should occur may not be experimentally well-defined due to significant nonlinearities prior and after the supposed switching in the behaviour (van Dommelen et al., 2003). (Micro)structural based models help alleviate this problem; however, they introduce other challenges. Of note is the inordinate number of parameters that these models often contain (Morovati et al., 2021; Xiao et al., 2021 and Uchida et al., 2022), which as noted by Zhan et al. (2023) and elegantly demonstrated by Ogden et al. (2004) for problems of nonlinear optimisation, puts into question the uniqueness of the obtained fits and model parameter values. Moreover, by nature, a microstructural model is developed for an intended certain structural composition, and thus may not be meaningfully applicable to polymers or elastomers with other types of structural configuration or components. Finally, it is often the case that the values of some or even many of those structural parameters are not independently known, since there is no structural data available to the required resolution for elucidating those values. Therefore, in those cases, the parameter values are either 'assumed' from the literature (as in Lee et al., 2020 serving as an example), or left to be determined by fitting to the deformation data. To this extent, such (micro)structural models may therefore not offer a particular advantage over the phenomenological models, but instead may come with the disadvantage of being computationally too expensive to implement and run. The literature also suggests that some of these (micro)structural models may not be able to capture the multiaxial deformation data (see, e.g., Khiêm and Itskov (2017) and Akbari et al. (2022) for discussions).

In light of the foregoing, I wish to put forward some criteria for defining a *suitable* model for application to the large deformation of various polymer types, encompassing both *elastic* and *inelastic* behaviours, as follows. A *suitable* model should be as simple as possible and as empirically successful as required. It must include a comprehensive set of constitutive parameters so as to allow capturing the elastic and inelastic behaviours of interest accurately, but with a reduced set of number of parameters so that the implementation and application of the model is versatile and efficient. The *elastic* and *inelastic* features of concern are, explicitly, the nonlinearity in the deformation behaviour, the peak stress followed by a drop, softening and/or plateau, and the final hardening phase before total fracture/failure. And, its applicability must be *inclusive*; i.e., the model must provide a degree of *universality* for application across various types of elastomers. The similarities between the inelastic behaviour of a wide range of polymers,

[1] Some of these 'inelastic' features may be attributed to phenomena such as initiation and propagation of necking etc. However, here I view these features as intrinsic constitutive behaviour of those polymers.

e.g., elastomeric, amorphous thermoplastic and semi-crystalline polymers, have been underlined in the works of Zaïri and co-workers (Ayoub et al., 2010; 2011; Cherief et al., 2020; Yan et al., 2021). The case for a unified model for applicability to these varied types of polymers is therefore well founded. Once the model successfully satisfies these attributes, and captures the foregoing behaviours in the (primary) loading path, it must also be straightforwardly amenable to extension for capturing the unloading and rate-dependent behaviours observed in the mechanical tests of polymers. It is the objective of this paper to present one such model and its application to published extant data from various types of elastomers with distinct elastic and inelastic behaviours. Meeting this objective forms the beginnings of the drive to move towards a *unified* model for application to the large deformation (elastic and inelastic) of polymers, at least at an empirical level. As the first step, here the focus is afforded on isothermal deformations, and the effects of temperature are unaccounted.

The view point I invoke in this endeavour, of proposing such a *suitable* model, is that (finite) deformations, be it in elastic and/or inelastic ranges, are associated with a deformation energy. Akin to what is customary in hyperleasticity, let us refer to that deformation energy as a generic strain energy, denoted by W. Note that such a strain energy need not be prescriptively restricted to a 'hyperelastic' material or a 'hyperelastic' deformation. The purpose of that strain energy function W, then, is only to relate the deformation energy to the deformation gradient, for the whole range of deformation including the elastic and inelastic ranges.[2] As such, the constitutive parameters of this energy function W should ideally determine and predict both the elastic and inelastic behaviours (in the primary loading path), without the need for additional damage or switch parameters etc. I refer to this deformation energy function W as the 'core' *hyperinelastic* energy function. The term 'hyperinelastic' signifies large deformations of both elastic and inelastic attributions, characterised via a unified deformation energy W. The word 'core' highlights that the *hyperinelastic* W function so referred only incorporates the effect of deformation; thus accounts for the elastic and inelastic behaviours arising only from the deformation, and *not* the temperature or rate etc effects. Discounting the thermal effects (as only isothermal deformations are at the centre of focus here), additional inelastic features such as discontinuous softening (in the unloading path) and rate-effects will be incorporated into the *core* hyperinelastic energy function W as an augmentation — this will be specified shortly in the next paragraph. The idea for postulating such a function draws inspiration from a recent work by the author, where the continuous softening (up to the point of failure) in the primary stress–deformation curves of a select set of soft materials was considered an intrinsic constitutive behaviour, captured by the constitutive parameters embodied within a comprehensive strain energy function (Anssari-Benam, 2023). Here, I wish to further generalise that concept, and to extend it so as to encompass the inelastic features specified earlier in the foregoing.

Accordingly, an exemplar core hyperinelastic deformation energy function W, based on a previous work (Anssari-Benam, 2024) will be presented in Section 2 and will be used for fitting with extant deformation datasets pertaining to elastic and inelastic behaviours of various elastomers. The fitting results will be presented in Section 3. Seven examples, specifically, will be considered in that section. Those include the whole-range (elastic and inelastic) large deformation of: (i–iii) open- and closed-cell polyurethane and closed-cell polystyrene foams under uniaxial compression due to Lee et al. (2020); (iv) poly(methyl methacrylate) specimens under tensile deformation, as an example of glassy polymers, due to Uchida et al. (2022); (v) a high density polyethylene sample under uniaxial deformation due to Ayoub et al. (2010) by way of exemplifying a semi-crystalline polymer; (vi) a quadruple-network hydrogel under uniaxial tension by Vernerey et al. (2018); and (vii) isotropic-genesis polydomain LCE specimens due to Tokumoto et al. (2021), considering only the uniaxial deformation. The modelling results will be presented, and a brief qualitative comparison with the elaborate models considered in the original studies will be provided, highlighting the improved quality of fits using the considered model in the current paper. The examples of application provided in Section 3 only include large quasi-static deformations in the primary loading path. In view of those successful applications, the considered core hyperinelastic energy function W will be augmented in Section 4 to capture the unloading behaviour. This extension will be made by incorporating a scalar discontinuous 'inelasticity' parameter, inspired by the work of Anssari-Benam et al. (2023) in relation to Mullins-like damage, into the core hyperinelastic deformation energy function W, providing a versatile tool for modelling the nonlinear unloading behaviour as well. The application of the model will then be presented for capturing the unloading behaviour of the same glassy, semi-crystalline and hydrogel polymer specimens of Uchida et al. (2022), Ayoub et al. (2010) and Vernerey et al. (2018), respectively. Favourable modelling results will be demonstrated. In Section 5, the rate of deformation will be incorporated into the considered *core* W model, using the framework recently proposed by Anssari-Benam and Hossain (2023), namely the evolution of model parameter with (a measure of) deformation rate. The application of the model to the rate-dependent behaviour of the same open- and closed-cell polyurethane and closed-cell polystyrene foams due to Lee et al. (2020) will be presented. Given the simplicity of the model, its applicability to capturing the elastic and inelastic behaviours under large deformations and across various polymer types, and the accuracy of the provided fits, the presented model is suggested as the foundation of a unified modelling tool for application to the elastic and inelastic finite deformation of polymers, by way of conclusion in Section 6.

2. The core *hyperinelastic* model

The core *hyperinealstic* deformation energy function W is defined as a mathematical function which relates the deformation energy to the deformation gradient $\mathbf{F}$; i.e., $W(\mathbf{F})$. Only to this extent, the said function has similarity with the customary strain

[2] The deformation energy is the area underneath the stress–deformation curve, over the whole range of deformation (encompassing both elastic and inelastic ranges), which is represented by the stipulated W function. No full recovery of the deformation or the deformation energy, upon the removal of the initial loading, is intended or required here.

energy function of hyperelasticity. However, here the deformation may span across both *elastic* and *inelastic* ranges. The contained constitutive parameters in the core *hyperinealstic* deformation energy function $W(\mathbf{F})$ are such that they determine and capture the inelastic behaviour too, as a natural progression to the (hyper)elastic phase. The intended elastic and inelastic behaviours to be captured by this core *hyperinealstic* function relate to the (primary) loading path, and no full recovery of the deformation or the energy is necessary or required upon the removal of the applied deformation.

The functional form of this core *hyperinealstic* energy $W(\mathbf{F})$ remains a judicious empirical choice, ideally based on mathematical and continuum mechanics axioms to ensure the robustness of the model, while the suitability of the model is ultimately determined by how well that functional choice captures and predicts the experimental data. Accordingly, and due to the reasons which will be explained shortly in the sequel, here the following function is considered[3]:

$$W(\mathbf{F}) \equiv W(I_1, I_2) = \sum_{i=1} \frac{3(n_i-1)}{2n_i}\mu_i N_i \left[\frac{1}{3N_i(n_i-1)}(I_1-3)^{\beta_i} - \ln\left(\frac{I_1-3N_i}{3-3N_i}\right)^{\beta_i}\right] + \sum_{k=1} C_k\left[\left(\frac{I_2}{3}\right)^{\epsilon_k} - 1\right], \tag{1}$$

where μ_i and C_k are stress-like and N_i, n_i, β_i and ϵ_k are dimensionless model parameters. Note that I_1 and I_2 are the first and second principal invariants of $\mathbf{B}(=\mathbf{F}\mathbf{F}^{\mathrm{T}})$, respectively. The infinitesimal shear modulus μ_0 for this model is:

$$\mu_0 = \sum_{i=1} \frac{\mu_i\beta_i N_i(1-n_i)}{n_i(1-N_i)} + \sum_{k=1} \frac{2\epsilon_k}{3}C_k\,. \tag{2}$$

This specific core *hyperinealstic* energy function $W(\mathbf{F})$ of binomial form is adopted here for the following reasons. First, as shown in Anssari-Benam (2024), this model has a demonstrable accurate applicability to hyperelastic deformations across various polymers and elastomers, ranging from natural and filled rubbers to hydrogels, foams, biomaterials and LCEs. To this end, the considered model in Eq. (1) is poised to provide a degree of *universality* for a general application to various soft solids. Second, its response functions W_1 and W_2, where subscripts 1 and 2 denote the partial derivative of W with respect to I_1 and I_2, are rooted in well-defined mathematical axioms. The response function W_1 is a general rational function of order $\lfloor\beta/1\rfloor$:

$$2W_1 = \sum_{i=1} \frac{1}{n_i}\mu_i\beta_i \frac{I_1(I_1-3)^{\beta_i-1} + 3N_i\left[1-(I_1-3)^{\beta_i-1}\right] - 3n_iN_i}{I_1-3N_i}, \tag{3}$$

while the response function W_2 is also a generalisation of the Carroll-type I_2 term (Carroll, 2011):

$$2W_2 = \sum_{k=1} \frac{2C_k\epsilon_k}{3^{\epsilon_k}} I_2^{\epsilon_k-1}\,. \tag{4}$$

As a result of its generalised form, the model in Eq. (1) is *parent* to most classical strain energy functions in the literature, from the neo-Hookean (Treloar, 1943), Yeoh (Yeoh, 1990) and Mooney–Rivlin (Rivlin, 1948) to the inverse Langevin-related models of Gent (1996) and Arruda and Boyce (1993) etc; i.e., those models are all a special sub-set of the model in Eq. (1). See Anssari-Benam (2024) for a demonstration and a more exhaustive list of models. Third, as will be shown in Section 3, the model embodies a comprehensive set of constitutive parameters which allows an accurate capturing of the deformation behaviour of a wide range of elastomers in the inelastic phase too, without the need of superimposing additional parameters or switches or conditions.

Following Mihai and Goriely (2011), here we further generalise the overtly prescriptive ranges for the model parameters that were originally designated in Anssari-Benam (2024), to:

$$\begin{cases} n_i, \mu_i, N_i \in \mathbb{R}^+\,, \\ \\ \beta_i, C_k, \epsilon_k \in \mathbb{R}\,. \end{cases} \tag{5}$$

This generalisation ensures that no mechanical behaviour, even those that are not the classically observed phenomena such as the negative Poynting effect (Mihai and Goriely, 2011) will not be excluded from the possible ranges that the model parameters may assume. While the model in Eq. (1) may be expanded to any number of terms desired, in this work expansions beyond two terms will not be considered; i.e., $i, k \leq 2$, to minimise the number of model parameters and thereby reduce the risk of non-uniqueness issues in finding the optimal fit and the model parameter values (Ogden et al., 2004).

The stress–deformation relationships for a given boundary value problem may be derived from the energy function $W(\mathbf{F})$ of Eq. (1) using the representation formula (Beatty, 1987):

$$\mathbf{T} = -p\,\mathbf{I} + 2W_1\,\mathbf{B} - 2W_2\,\mathbf{B}^{-1}\,, \tag{6}$$

where $\mathbf{T}$ is the (principal) Cauchy stress, $\mathbf{B}$ is the left Cauchy–Green deformation tensor and $\mathbf{B}^{-1}$ is its inverse, p is the arbitrary Lagrange multiplier enforcing the condition of incompressibility, and $\mathbf{I}$ is the identity tensor. Since, as will be seen in the sequel, the primary loading mode employed in the literature to investigate and characterise the inelastic behaviour of polymers is uniaxial deformation, here it suffices to derive the ensuing stress–stretch relationship only for the uniaxial deformation on using the model

[3] The theoretical analysis throughout this work is carried out within the assumption of incompressibility.

in Eq. (1). Considering that in uniaxial deformation we have $\lambda_1 = \lambda$ and $\lambda_2 = \lambda_3 = \lambda^{-0.5}$, and under the assumption of plane stress $(T_{33} = 0)$, we find from Eqs. (1) and (6):

$$T_{uni} = \sum_{i=1} \frac{\mu_i \beta_i}{n_i} \frac{I_1 \left(I_1 - 3\right)^{\beta_i - 1} + 3N_i \left[1 - \left(I_1 - 3\right)^{\beta_i - 1}\right] - 3n_i N_i}{I_1 - 3N_i} \left(\lambda^2 - \frac{1}{\lambda}\right) + \sum_{k=1} \frac{2C_k \epsilon_k}{3^{\epsilon_k}} I_2^{\epsilon_k - 1} \left(\lambda - \frac{1}{\lambda^2}\right). \tag{7}$$

Note that $I_1 = \lambda^2 + 2\lambda^{-1}$ and $I_2 = 2\lambda + \lambda^{-2}$. This relationship will be used in Section 3 for fitting with the experimental data of elastic and inelastic behaviours of a variety of polymers in the (primary) loading path.

3. Application to experimental data

In this section, the application of the core *hyperinelastic* model in Eq. (1) will be considered to the elastic and inelastic behaviours of various polymeric specimens, as published in the literature. These include polymer foam specimens of Lee et al. (2020), glassy polymer samples due to Ames et al. (2009) as reported in Uchida et al. (2022), semi-crystalline polymer samples of Ayoub et al. (2010), multi-network hydrogel specimens as used by Vernerey et al. (2018), and polydomain LCEs due to Tokumoto et al. (2021). The sequential elastic and inelastic behaviours of these exemplar polymers/elastomers will be considered and modelled in the primary loading path under uniaxial deformation, as reported in those studies. The correlation between the model and the experimental data for each case will be presented in the following subsections. The adaptation for, and application to, the unloading behaviour will be presented in Section 4.

The modelling is performed by fitting the (Cauchy)stress–stretch relationship in Eq. (7) to each considered dataset. Depending on the goodness of fit, either one term (i.e., $i = k = 1$) or two-term (i.e., $i = k = 1, 2$) expansions of the model will be considered, correlating with one-term or two-term forms of the stress–stretch relationship in Eq. (7). The optimal fit is obtained by minimising the residual sum of squares (RSS) function defined as: $\text{RSS} = \sum_x \left(T^{model} - T^{experiment}\right)_x^2$, where x is the number of datapoints and T is the Cauchy stress. The minimisation is performed via an in-house developed code in MATLAB®, using the genetic algorithm (GA) function. The datapoint in the undeformed state, i.e., $(\lambda = 1, T = 0)$, was removed from each dataset before the fitting process in order to eliminate the numerical instabilities that may arise in cases when $\beta < 1$; i.e., to avoid division by zero at point $\lambda = 1$. The coefficient of determination R^2 values are reported as a measure of the goodness of the obtained fits.

3.1. Polymer foams

We start the modelling campaign with the elastic and inelastic behaviours of a polymeric foam sample. Lee et al. (2020) present a detailed set of data on uniaxial compression of open- and closed-cell[4] polyurethane, and closed-cell polystyrene foams. Their dataset is particularly interesting as it employs compression tests. The customary mode of deformation in the literature is uniaxial tension, and as a result the performance of the many of the existing models in the literature remains untested for capturing the inelastic behaviour under compression. This is particularly important since in most polymers, the tension–compression behaviour is asymmetric. Therefore, if a model is seen to capture the tensile behaviour, there is no guarantee that the said model may be suitably applied to the compression behaviour as well. The modelling results for these three specimens are shown in Fig. 1, and Table 1 summarises the identified model parameter values. The tabulated numerical datapoints for this dataset has been provided in Appendix, Table A.1.

The model is seen to capture the elastic and inelastic behaviours favourably, with R^2 values in excess of 0.99. Note that for the closed-cell polyurethane and polystyrene foam specimens, Figs. 1(a) and (b), respectively, the two-term expansion of the model was considered, while it was observed empirically that the one-term expansion was suitable for the open-cell polyurethane sample (Fig. 1c). The model captures the initial elastic behaviour, as well as the inelastic behaviours which for each of the three samples are distinct. The relative error plots for each dataset, calculated as: $\left|\frac{T^{experiment} - T^{model}}{T^{experiment}}\right| \times 100$, are provided in Fig. 2.

For the closed-cell polyurethane specimen, the inelastic phase proceeds after reaching a peak stress, followed by softening and a plateau-like behaviour, leading to a final hardening phase — see the plot in Fig. 1(a). The model is seen to capture this challenging inelastic behaviour well, and in particular the peak-and-trough of the plateau phase as well as the hardening behaviour are emulated successfully. It is interesting to note that by changing the value of the model parameter N_1, the peak behaviour could be better captured as well — see the plots in Fig. 1(d) which illustrate the effect of increasing N_1 values on capturing the peak stress.

The inelastic behaviour of the closed-cell polystyrene foam sample is seen to be slightly different to that of the previous specimen — see Fig. 1(b). The peak behaviour here is less pronounced, and the plateau pahse is considerably shorter. The hardening behaviour, however, is longer and has a more complex shape than the former. With this varied behaviour, the model is again seen to capture the elastic and inelastic responses most favourably.

Finally, the deformation behaviour of the open-cell polyurethane sample is distinct from the former two specimens. As the plot in Fig. 1(c) demonstrates, here there is no discernible feature of inelasticity, and the stress–stretch curve is reminiscent of a continuous behaviour up to the hardening region. Nonetheless, the model is seen to successfully capture the behaviour of this specimen too.

[4] These refer to the microstructural morphology of the specimens.

Table 1
Model paramter values for the elastic and inelastic behaviour of polymeric foam specimens due to Lee et al. (2020).

Closed-cell polyurethane					
μ_1 [MPa]	N_1 [–]	n_1 [–]	β_1 [–]	C_1 [MPa]	ϵ_1 [–]
3.01	0.99_8	0.94	1.05	−0.95	−4.91
μ_2 [MPa]	N_2 [–]	n_2 [–]	β_2 [–]	C_2 [MPa]	ϵ_2 [–]
0.11	0.99_9	11.52	0.72	16.70	−0.09
Closed-cell polystyrene					
μ_1 [MPa]	N_1 [–]	n_1 [–]	β_1 [–]	C_1 [MPa]	ϵ_1 [–]
0.27	0.41	0.52	0.99_7	-1.04_5	-0.95_5
μ_2 [MPa]	N_2 [–]	n_2 [–]	β_2 [–]	C_2 [MPa]	ϵ_2 [–]
0.37	0.99_8	0.99_7	1.59	−9.90	0.18
Open-cell polyurethane					
μ [MPa]	N [–]	n [–]	β [–]	C [MPa]	ϵ [–]
0.97	0.08	8.98	0.91	0.17	−0.17

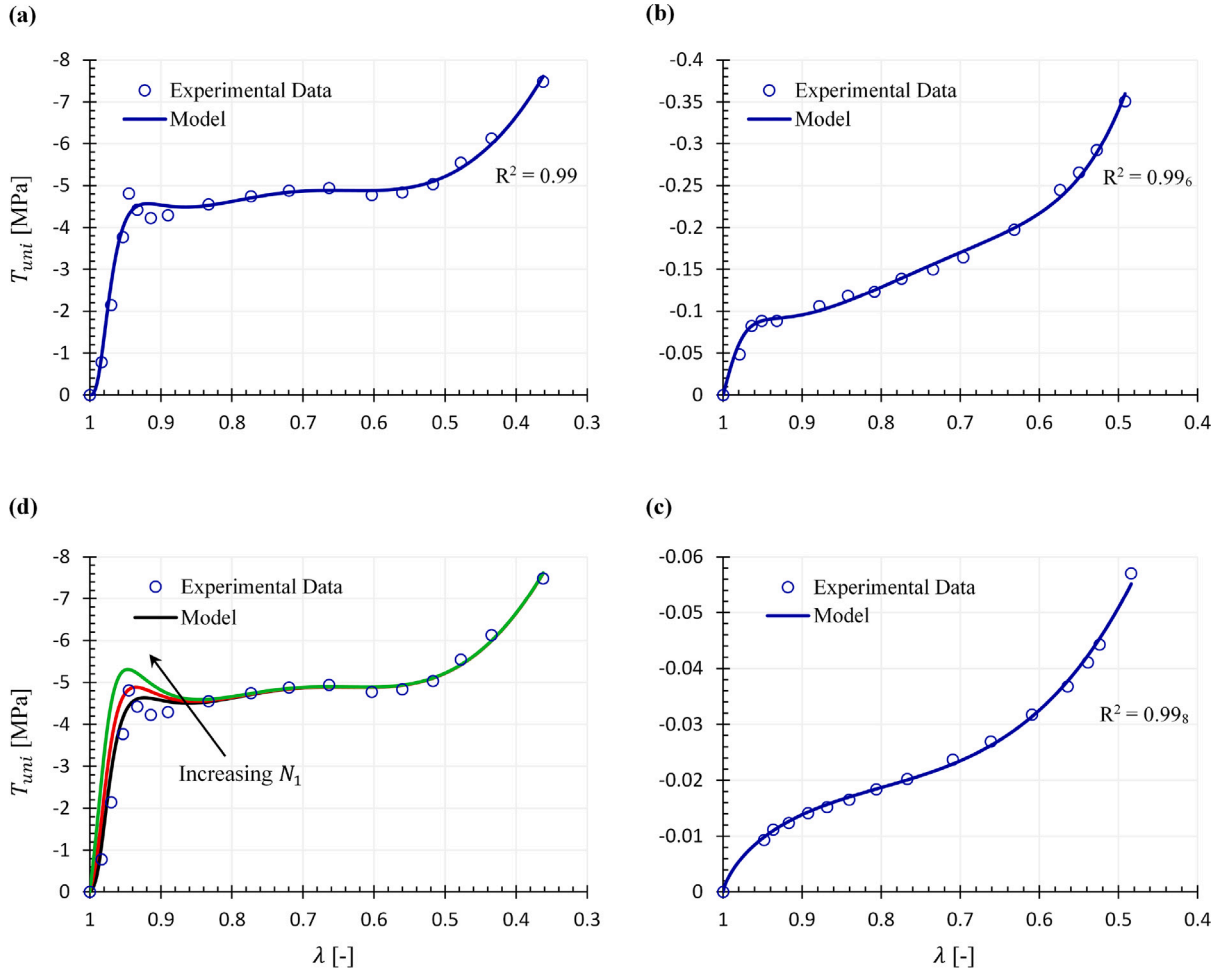

Fig. 1. Modelling results of the elastic and inelastic behaviour of polymeric foam specimens due to Lee et al. (2020) under uniaxial compression: (a) closed-cell polyurethane; (b) closed-cell polystyrene; and (c) open-cell polyurethane foams. R^2 values pertaining to the fits have been provided in each panel. Panel (d) shows the possibility of capturing the peak stress with more accuracy upon varying only one of the model parameter values, namely that of N_1, with respect to the optimal fit value (given in Table 1). The values of N_1 here vary between $0.998 < N_1 < 1$. Note that panels (a) to (d) have been designated in clock-wise order. The scale of the coordinate axes in the panels are different for a better clarity of presentation.

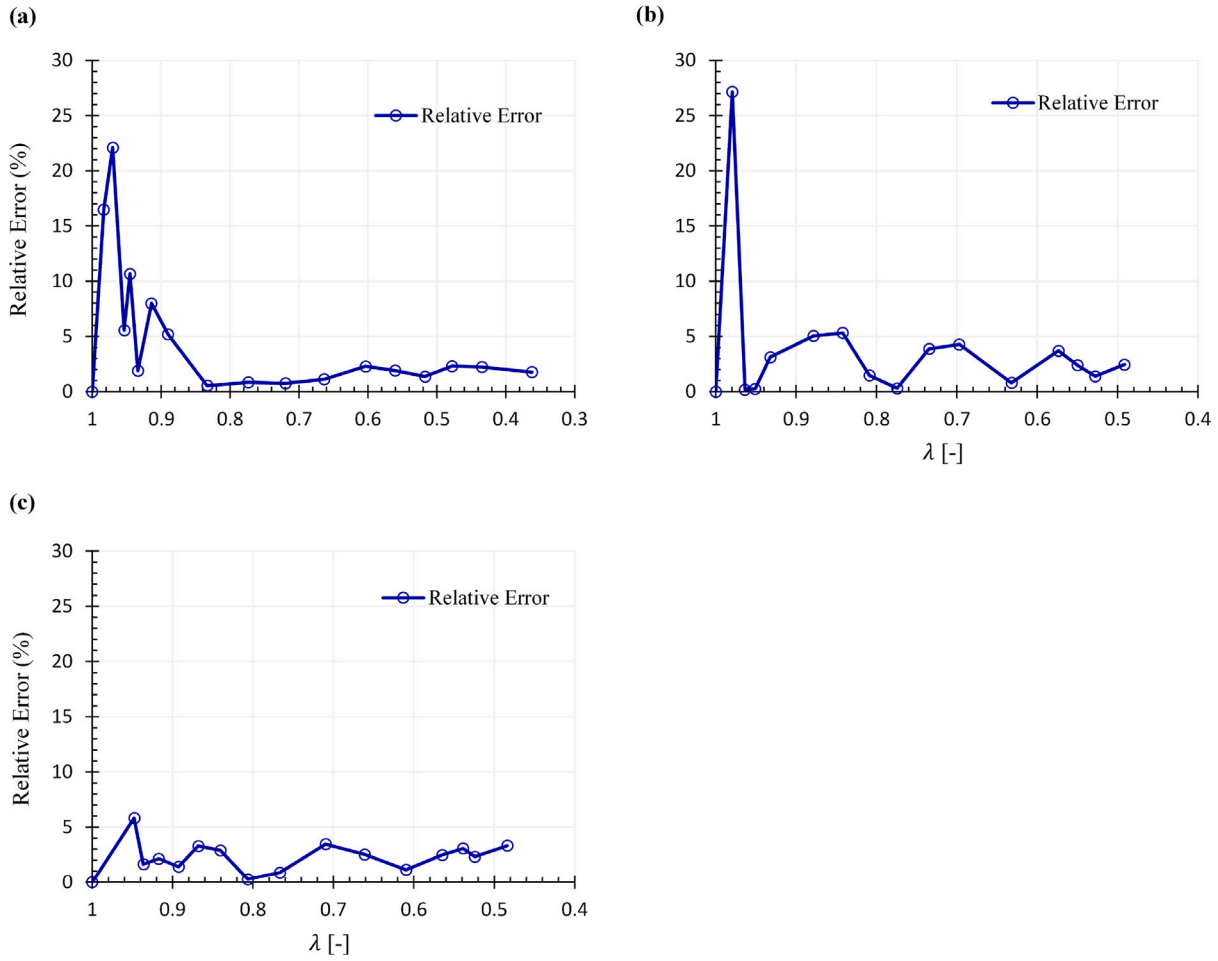

Fig. 2. The relative error plots for the Lee et al. (2020) dataset using the proposed *hyperinelastic* model: (a) closed-cell polyurethane; (b) closed-cell polystyrene; and (c) open-cell polyurethane foam specimens. Except for the initial small deformations, the relative errors are typically below 5%. Note that the scale of the x axis in the panels are different, consistent with the deformation range for each sample.

To better appreciate the versatility of the considered *hyperinelastic* model in this work and the accuracy of the obtained modelling results, it may be informative to recall that for modelling the same datasets, Lee et al. (2020) employed modified versions of two previously proposed models in literature, e.g., Tvergaard (1981) and Khan et al. (2004), containing 15 and 19 model parameters, respectively. A qualitative comparison between their obtained modelling results, Figures 10, 13 and 14 therein, and those of Fig. 1 here indicates the better accuracy of the model in Eq. (1), particularly for the deformation of the open-cell polyurethane specimens.

3.2. Glassy polymers

As an exemplar sample for glassy polymers, the dataset of Ames et al. (2009) is considered here, utilised by Uchida et al. (2022), which reports on the uniaxial tension of a poly(methyl methacrylate) specimen. The one-term form of the model was observed to be sufficient for capturing this dataset. The modelling result is provided in Fig. 3(a), and the identified model parameter values are listed in Table 2. The numerical datapoints, collated from Uchida et al. (2022), have been tabulated in Appendix, Table A.2.

Table 2
The identified model paramter values for the elastic and inelastic behaviour of the poly(methyl methacrylate) specimen due to Ames et al. (2009), on using the one-term expansion of the proposed model.

μ [MPa]	N [–]	n [–]	β [–]	C [MPa]	ϵ [–]
33.13	0.99_5	0.85	0.71	3.18_5	5.22

Both elastic and inelastic behaviours of this specimen are seen to possess distinct features than those of polymeric foams presented in the preceding section. The initial ‘elastic’ phase has a more pronounced nonlinearity, and inelastic phase consists of a softening

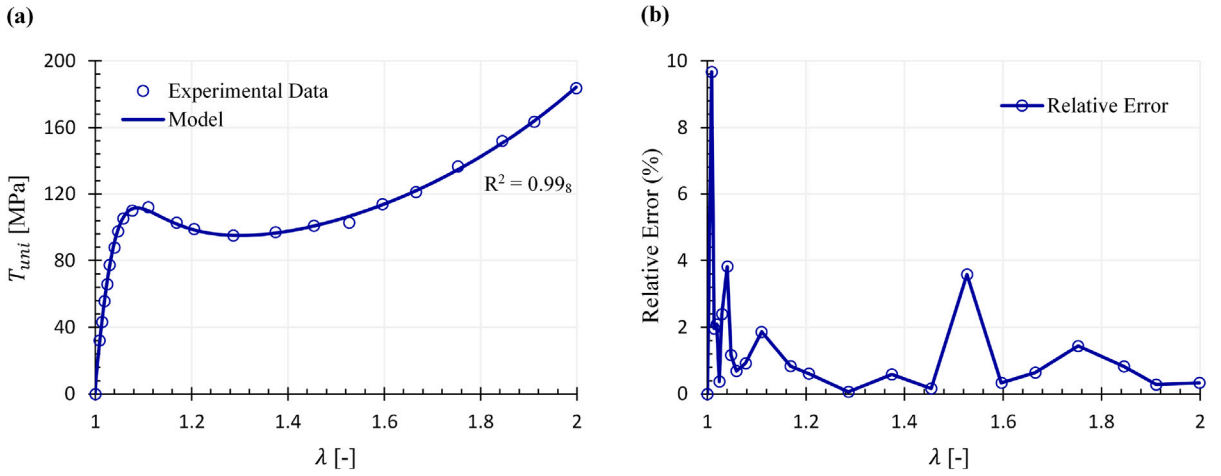

Fig. 3. Modelling results for the poly(methyl methacrylate) specimen of Ames et al. (2009), as reported in Uchida et al. (2022): (a) the fitting of the one-term expansion of the model with the data; and (b) the ensuing relative errors, typically below 4%.

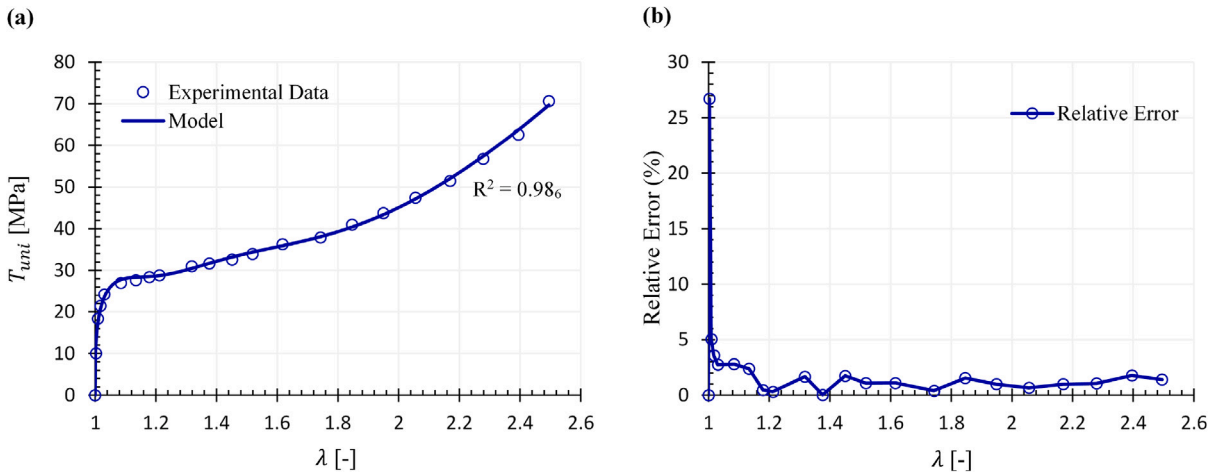

Fig. 4. Modelling results for the deformation of the semi-crystalline polymer samples of Ayoub et al. (2010): (a) the fitting of the two-term expansion of the model with the data; and (b) the ensuing relative errors, typically below 5%.

(i.e., drop in stress) after the peak behaviour, followed by a hardening response. The one-term expansion of the model captures these features most favourably (see Fig. 3), with R^2 in excess of 0.99. The relative error plot for this dataset has been given in Fig. 3(b). It is seen that except for the initial part of the deformation, the relative errors are typically below 4%.

It may be instructive to note that when the 24-parameter model used by Uchida et al. (2022) was fitted to this dataset, the model overshot the peak stress and underestimated the hardening behaviour considerably. See the modelling results in Figure 18 therein. While the 6-paramter model here may not capture all the effects embedded in that model, most notably the effect of temperature, the versatility and accuracy that the *hyperinelastic* model here offers may be deemed advantageous.

3.3. Semi-crystalline polymers

The high density polyethylene samples of Ayoub et al. (2010) are considered here as an example for the deformation behaviour of semi-crystalline polymers. The Ayoub et al. (2010) dataset reports on the uniaxial tensile deformation of those specimens. The tabulated numerical values of this dataset are provided in Table A.3 of Appendix. It was empirically ascertained that the two-term expansion of the model more suitably captures this dataset. Accordingly, the two-term form of the model in Eq. (7) was fitted to this data. The modelling results, along with the relative error plot, are presented in Fig. 4. Table 3 contains the obtained model parameter values.

Table 3
The identified model parameter values for the elastic and inelastic deformations of high density polyethylene samples due to Ayoub et al. (2010).

μ_1 [MPa]	N_1 [–]	n_1 [–]	β_1 [–]	C_1 [MPa]	ϵ_1 [–]
31.23	0.65	0.57	0.66	50.00	−0.49
μ_2 [MPa]	N_2 [–]	n_2 [–]	β_2 [–]	C_2 [MPa]	ϵ_2 [–]
50.00	0.86	10.00	0.71	−50.00	−4.61

The elastic and inelastic behaviours of this specimen distinctly differ from those of the glassy polymer sample in the previous section. As can be seen in the plots of Fig. 4(a), the specimens exhibit a rapid nonlinear initial deformation, reaching a plateau and followed by a bi-phasic hardening; namely a seemingly linear hardening behaviour leading to a nonlinear hardening phase. The proposed *hyperinelastic* model of Eq. (1), in its two-term expansion form, successfully captures these behaviours, with R^2 value in excess of 0.98. The point-wise relative error plot has also been provided in Fig. 4(b). Similar to the previous examples, except for the initial (small) range of deformation, the value of the relative error is below 5%.

For a qualitative understanding of the challenging nature of modelling this dataset, it may be worth noting that the model used by Ayoub et al. (2010), with 21 model parameters, notably underestimated the plateauing behaviour, while overshooting the hardening phase. See, for example, Figure 11 therein. The better accuracy and versatility of the current model in capturing this dataset is tangible.

3.4. Hydrogels

Vernerey et al. (2018) present an interesting dataset of a quadruple-network hydrogel specimen under uniaxial tension. Unlike the classical double- or triple-network hydrogels, this specimen shows a rapid initial nonlinear hardening, reaching a peak stress, followed by a softening (i.e., drop in the stress) and plateau, eventually leading to a final hardening phase — see the plot in Fig. 5. Here we undertake to model these inelastic features with the proposed *hyperinelastic* model of Eq. (1). On using the two-term expansion of the model, the fitting results are shown in Fig. 5(a). The identified model parameter values have been listed in Table 4. The numerical values of the datapoints collated from Vernerey et al. (2018) have been given in Table A.4 of Appendix.

Table 4
Model parameter values for the deformation behaviour of the quadruple-network hydrogel specimens of Vernerey et al. (2018).

μ_1 [MPa]	N_1 [–]	n_1 [–]	β_1 [–]	C_1 [MPa]	ϵ_1 [–]
0.12	0.96	0.80	0.65	11.41	−3.58
μ_2 [MPa]	N_2 [–]	n_2 [–]	β_2 [–]	C_2 [MPa]	ϵ_2 [–]
0.11	0.96	0.62	0.99_9	−16.06	−2.46

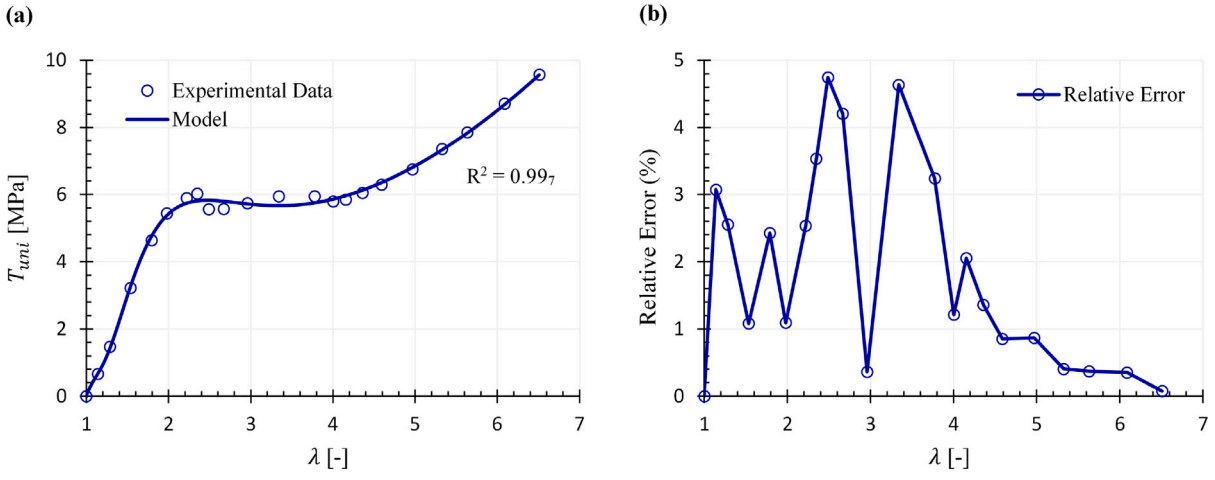

Fig. 5. Modelling results for the uniaxial tension of the quadruple-network hydrogel samples due to Vernerey et al. (2018): (a) the fitting of the two-term expansion of the model with the data; and (b) the ensuing relative errors, remaining below 5% throughout the whole deformation range.

Similar to the previous examples, the model is seen to capture the elastic and inelastic behaviours of the specimen favourably, with a R^2 value in excess of 0.99. The relative error plot in Fig. 5(b) further reinforces this successful capturing of the data, as the relative error values remain below 5% throughout the deformation range.

For the purpose of a qualitative comparison, the reader is reminded that the complex structural-based model proposed in Vernerey et al. (2018) for capturing the finite deformation behaviour of this specimen, with excessive number of model parameters, overshoots the softening/plateau region and underestimates the hardening behaviour — see Figure 9 therein for a comparison. The improved accuracy in capturing this dataset by the considered model here is noticeable.

3.5. Polydomain LCEs

As the final example, and to bring to the attention of the reader the variety of elastomer types in the application of the proposed model, here the dataset from Tokumoto et al. (2021) is considered which reports on the large deformation of polydomain[5] LCEs. For the purpose of the current work, here we only consider the uniaxial deformation data. For the application of the model to the multiaxial dataset, the interested reader may wish to refer to Anssari-Benam et al. (2024). The tabulated numerical datapoints of this dataset has also been presented therein.

While strictly not an inelastic behaviour, the 'soft elasticity' plateau in the stress–deformation curves of LCEs has similarities with the softening behaviour examples considered in the preceding subsections, and poses a challenge to the existing models for capturing this behaviour. To keep the modelling approach simple, and for presentation purposes only, here we show the application of the one-term model to the uniaxial deformation data of Tokumoto et al. (2021). The plots in Fig. 6 present the modelling results, and Table 5 summarises the model parameter values.

Table 5
The obtained model paramter values for the uniaxial deformation of polydomain LCE samples due to Tokumoto et al. (2021), on using the one-term expansion of the proposed model.

μ [kPa]	N [–]	n [–]	β [–]	C [kPa]	ϵ [–]
7.28	0.93	0.48	1.11	226.62	−0.45

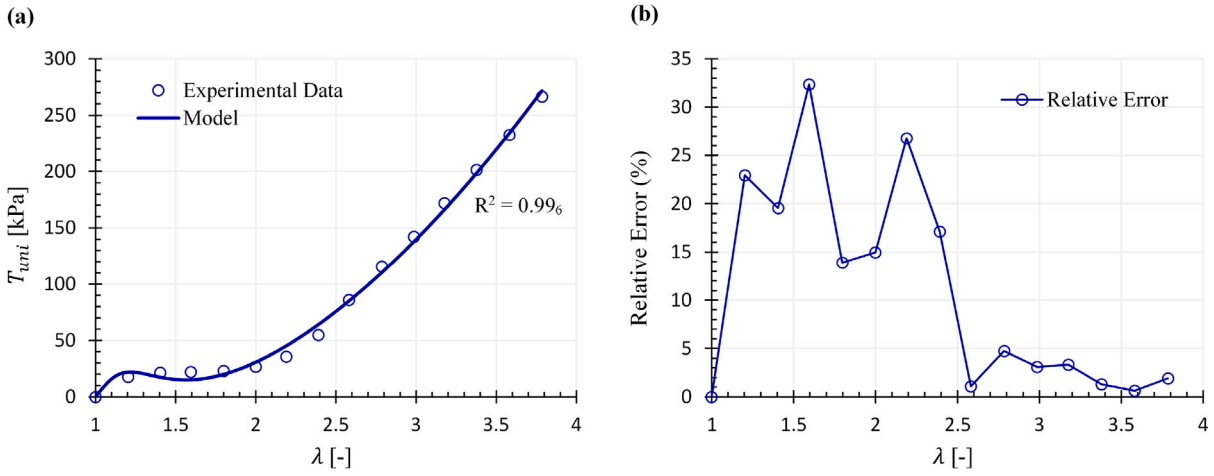

Fig. 6. Modelling results for the uniaxial tensile deformation of the polydomain LCE specimens of Tokumoto et al. (2021): (a) the fit obtained on using the one-term form of the model; and (b) the ensuing relative errors.

As the results indicate, the soft elasticity behaviour is captured favourably, even via the simplest (one-term) form of the model. The R^2 value is in excess of 0.99. For comparison, the reader is reminded that to capture the behaviour of these samples, an elaborate multi-variable discrete model, discretised over various ranges of deformation in the stress–strain curve to capture each phase separately, was devised in Tokumoto et al. (2021). Although that model was applied therein to the multiaxial deformation of the specimens, the simplicity and accuracy of the current modelling approach offers a versatile and useful alternative. While not pursued here, the application of the proposed model here to the multiaxial deformation of those specimens can be found in Anssari-Benam et al. (2024).

[5] Polydomain LCEs possess a macroscopically isotropic mechanical behaviour.

4. Modelling the unloading behaviour

As the presented examples in Section 3 demonstrated, the continuous progression of the inelastic behaviour from the elastic range of deformation, in the primary loading stress–deformation curve, is favourably captured by the proposed *hyperinelastic* model, without the need for superimposition of the customary damage functions, yield/flow limits and switches, or other dissipative provisions. However, an important manifestation of inelastic behaviour also reflects itself in the unloading path, when the loading stimuli are removed and the specimen is allowed to return to, say, a stress-free configuration.

To that end, the unloading path exhibits a softening behaviour with respect to the loading curve, and depending on the structural composition of the subject specimen and the strength of the its recoil, may leave a permanent set as well. The amount of softening, the unloading response and the magnitude of the permanent set are thought to be primarily determined by the value of maximum deformation achieved in the preceding loading path. By nature, therefore, this softening behaviour is discontinuous, in that it is only reflected in the unloading path, and is often referred to as discontinuous damage (e.g., Ehret and Itskov, 2009).

Accordingly, in modelling the inelasticity reflected by the unloading behaviour in isothermal deformations here, one is guided by the following considerations: (i) since the proposed *hyperinelastic* model captures the continuous inelasticity of the loading path, the parameter(s) representing the inelasticity in the unloading path(s) must only be activated in the unloading path(s), rendering the primary loading stress–deformation curve unaffected; and (ii) the discontinuous inelasticity in the loading path(s) is governed by (a measure of) the maximum deformation experienced by the continuum prior to the initiation of unloading. A general modelling framework which is based on the foregoing requirements has been presented in Anssari-Benam et al. (2023), within the context of pseudo-elasticity (Ogden and Roxburgh, 1999). However, in order to achieve a better applicability in regards to inelasticity, that modelling framework is further adapted here, and will be incorporated into the considered *hyperinelastic* model for application to the experimental data in the sequel.

4.1. Discontinuous inelastic parameter

In the spirit of Anssari-Benam et al. (2023), we define a discontinuous inelasticity variable Ω as:

$$\Omega = \frac{1}{3}\sum_{j=1}^{3}\Omega_j\,, \tag{8}$$

where Ω_j $(j=1,2,3)$ may be seen as directional inelasticity variables[6] in the principal directions of deformation, that are considered to depend on the maximum value of the principal stretches λ_j reached in the *history* of loading before the initiation of unloading; $\Omega_j \equiv \Omega_j\left(\lambda_j^{max}\right)$. The functional form of this dependence is considered to be via a sigmoid-type function:

$$\Omega_j = \frac{b\left(\lambda_j^{max}\right)+2}{b\left(\lambda_j^{max}\right)+1} - \frac{1}{b\left(\lambda_j^{max}\right)+\exp\left\{-c\left(\lambda_j^{max}\right)\left[\lambda_j^{max}-\lambda_j\right]\left[\lambda_j^{max}-1\right]\right\}}. \tag{9}$$

Here, $b(\bullet)$ and $c(\bullet)$ are scalar functions of λ_j^{max}. Note that in each unloading cycle, the value of λ_j^{max} is constant, and as such $b\left(\lambda_j^{max}\right)$ and $c\left(\lambda_j^{max}\right)$ are single valued parameters in each unloading cycle. In the interest of better clarity, some remarks may be in order at this juncture.

Remark 1. The discontinuous inelasticity variable Ω is bounded within the range: $0<\Omega\leq 1$.

Remark 2. In principal direction(s) where deformation is compressive, i.e., $\lambda_j<1$, it is clear that $\lambda_j^{max}=1$. Therefore, from Eq. (9), Ω_j in those directions will be: $\Omega_j=1$.

Remark 3. In the primary loading path, for non-compressive principal deformation direction(s), at each point of deformation one has: $\lambda_j^{max}=\lambda_j$. As a result, from Eq. (9), we will again have $\Omega_j=1$. Due to Remark 2, for compressive principal deformation direction(s) we also have $\Omega_j=1$. Thus, in the primary loading path, one always has: $\Omega_j=1$, $j=1,2,3$, and from Eq. (8) it follows that $\Omega=1$.

The discontinuous inelasticity variable Ω, defined via Eqs. (8) and (9), shall now be incorporated into the core hyperinelastic function $W(\mathbf{F})$ of Eq. (1), to provide an 'augmented' hyperinelastic energy function denoted by $\widetilde{W}$, to facilitate the capturing of discontinuous inelasticity as well:

$$\widetilde{W} \equiv W(\mathbf{F},\Omega) = W\left(I_1,I_2,\Omega_j\right)\,. \tag{10}$$

[6] No structural interpretation is ascribed to Ω_j. As far as this work is concerned, Ω_j are phenomenological parameters.

In order to enable an explicit functional dependence of W on I_1, I_2 and Ω_j, it may be convenient to introduce the following change of variables:

$$\Gamma_j = \Omega_j^{\kappa\left(\lambda_j^{max}\right)}\lambda_j\,, \quad j=1,2,3, \tag{11}$$

where Γ_j may be viewed as 'pseudo-stretches' that have the effect of discontinuous inelasticity incorporated in them via $\kappa\left(\lambda_j^{max}\right)$, which acts as a modulating factor in converting the amount of inflicted inelasticity into residual stretch(es). The function $\kappa(\bullet)$ is a scalar function of λ_j^{max}, and similar to $b(\bullet)$ and $c(\bullet)$ of Eq. (9), is a single valued parameter in each unloading cycle.

Remark 4. Note that in the primary loading path $\Omega_j = 1$, and thus $\Gamma_j = \lambda_j$; i.e., there is no effect of discontinuous inelasticity in the primary loading curve.

Remark 5. When there is no permanent set, the exponent $\kappa\left(\lambda_j^{max}\right) = 0$ *a priori*, and again one has $\Gamma_j = \lambda_j$.

Accordingly, on using the definition of Γ_j in Eq. (11), the pseudo-invariants $\tilde{I}_1$ and $\tilde{I}_2$ may be defined as:

$$\begin{cases} \tilde{I}_1 = \Gamma_1^2+\Gamma_2^2+\Gamma_3^2 = \Omega_1^{2\kappa\left(\lambda_j^{max}\right)}\lambda_1^2+\Omega_2^{2\kappa\left(\lambda_j^{max}\right)}\lambda_2^2+\Omega_3^{2\kappa\left(\lambda_j^{max}\right)}\lambda_3^2\,, \\ \tilde{I}_2 = \Gamma_1^{-2}+\Gamma_2^{-2}+\Gamma_3^{-2} = \Omega_1^{-2\kappa\left(\lambda_j^{max}\right)}\lambda_1^{-2}+\Omega_2^{-2\kappa\left(\lambda_j^{max}\right)}\lambda_2^{-2}+\Omega_3^{-2\kappa\left(\lambda_j^{max}\right)}\lambda_3^{-2}\,, \end{cases} \tag{12}$$

where the following relationships hold:

$$\frac{\partial\tilde{I}_1}{\partial\Gamma_j} = 2\Gamma_j\,, \quad \frac{\partial\tilde{I}_2}{\partial\Gamma_j} = -2\Gamma_j^{-3}\,. \tag{13}$$

It follows that the 'augmented' hyperinelastic function of Eq. (10) now takes the form:

$$\widetilde{W} \equiv W(\mathbf{F},\Omega) \equiv W\left(I_1,I_2,\Omega_j\right) = W\left(\tilde{I}_1,\tilde{I}_2\right)\,, \tag{14}$$

or in explicit functional form as:

$$\widetilde{W} \equiv W\left(\tilde{I}_1,\tilde{I}_2\right) = \sum_{i=1}^{3}\frac{3\left(n_i-1\right)}{2n_i}\mu_i N_i\left[\frac{1}{3N_i\left(n_i-1\right)}\left(\tilde{I}_1-3\right)^{\beta_i}-\ln\left(\frac{\tilde{I}_1-3N_i}{3-3N_i}\right)^{\beta_i}\right]+\sum_{k=1}^{}C_k\left[\left(\frac{\tilde{I}_2}{3}\right)^{\epsilon_k}-1\right]\,. \tag{15}$$

It has been shown by Anssari-Benam et al. (2023) that the principal Cauchy stress components T_j are calculated from a deformation energy function $\widetilde{W}$, so defined via $W(\mathbf{F},\Omega)$, as:

$$T_j = \Omega\,\Gamma_j\frac{\partial\widetilde{W}}{\partial\Gamma_j}-p\,, \quad j=1,2,3. \tag{16}$$

On using the chain rule and the results in Eq. (13), the representation formula for the Cauchy stress in Eq. (6) may be re-written in terms of the pseudo-invariants $\tilde{I}_1$ and $\tilde{I}_2$ as:

$$T_j = \Omega\left[2\Gamma_j^2\frac{\partial\widetilde{W}}{\partial\tilde{I}_1}-2\Gamma_j^{-2}\frac{\partial\widetilde{W}}{\partial\tilde{I}_2}\right]-p\,, \quad j=1,2,3, \tag{17}$$

which, under the assumption of plane stress $\left(T_{33}=0\right)$ becomes:

$$T_j = \Omega\left[2\frac{\partial\widetilde{W}}{\partial\tilde{I}_1}\left(\Gamma_j^2-\Gamma_3^2\right)-2\frac{\partial\widetilde{W}}{\partial\tilde{I}_2}\left(\Gamma_3^{-2}-\Gamma_j^{-2}\right)\right]\,, \quad j=1,2,3. \tag{18}$$

For any given boundary value problem, e.g., uniaxial, biaxial, pure/simple shear etc deformations, the related stress–deformation relationships may be explicitly derived from the augmented hyperinelastic function $\widetilde{W}$ of Eq. (15), on using Eq. (18). What remains to do, prior to that step, is to specify the explicit functional forms of $b\left(\lambda_j^{max}\right)$, $c\left(\lambda_j^{max}\right)$ and $\kappa\left(\lambda_j^{max}\right)$. Such a designation remains, at this point, an empirical choice. An expedient option may be to consider a general three-parameter exponential function of the form:

$$\begin{cases} b\left(\lambda_j^{max}\right) = m_1\exp\left[m_2\left(\lambda_j^{max}\right)^{m_3}\right], \\ c\left(\lambda_j^{max}\right) = m_4\exp\left[m_5\left(\lambda_j^{max}\right)^{m_6}\right], \\ \kappa\left(\lambda_j^{max}\right) = m_7\exp\left[m_8\left(\lambda_j^{max}\right)^{m_9}\right], \end{cases} \tag{19}$$

where, m_z ($z = 1,..,9$) are dimensionless parameters and, in general, $m_z \in \mathbb{R}$. Overall, therefore, to also capture the discontinuous inelastic behaviour in the unloading path, the augmented hyperinelastic function $\widetilde{W}$ of Eq. (15) contains nine additional parameters to the *core* hyperinelastic function of Eq. (1), as given by Eq. (19).

The adaptation presented here extends the framework of Anssari-Benam et al. (2023), by allowing the parameters b, c and κ to be functions of the λ_j^{max} of each unloading cycle, instead of assuming a constant value in all unloading cycles. The assumption of constant b, c and κ values across all unloading cycles may be deemed more appropriate for a Mullins-like unloading behaviour, as in Anssari-Benam et al. (2023), and not for when large inelastic deformations are involved as in the current study. This extension, however, does not affect the derivation of the representation formula for the Cauchy stress, Eq. (16), or the thermodynamics consistency of the framework, which have been presented in detail elsewhere (e.g., Anssari-Benam et al., 2023; Anssari-Benam and Hossain, 2023).

4.2. Correlation with experimental data

In this section the application of the augmented hyperinelastic model in Eq. (15) to extant experimental datasets will be presented. As was the case with the primary loading path tests, the inelastic unloading behaviour of polymers appears to have been mainly investigated under uniaxial deformation mode in the literature. For the case of the examples considered here, the unloading datasets are taken from the studies presented in Section 3, where the *core* hyperinelastic model parameters of the primary loading path have been already established and presented. Here, therefore, by keeping those parameter values constant, we undertake to fit the augmented hyperinelastic model of Eq. (15) only to the unloading data, allowing the quantification of the parameters m_z ($z = 1,..,9$).

Accordingly, for uniaxial deformation we have the usual kinematics $\lambda_1 = \lambda$ and $\lambda_2 = \lambda_3 = \lambda^{-0.5}$. It is therefore clear that $\lambda_2^{max} = \lambda_3^{max} = 1$, and following Remark 2, then, $\Omega_2 = \Omega_3 = 1$. The ensuing $T_{uni} - \lambda$ using the augmented hyperinelastic function in Eq. (15) and the representation formula Eq. (18) becomes:

$$T_{uni} = \Omega\left\{\sum_{i=1}^{}\frac{\mu_i\beta_i}{n_i}\frac{\tilde{I}_1\left(\tilde{I}_1-3\right)^{\beta_i-1}+3N_i\left[1-\left(\tilde{I}_1-3\right)^{\beta_i-1}\right]-3n_iN_i}{\tilde{I}_1-3N_j}\left(\Omega_1^{2\kappa(\lambda^{max})}\lambda^2-\frac{1}{\lambda}\right)+\sum_{k=1}^{}\frac{2C_k\epsilon_k}{3^{\epsilon_k}}\tilde{I}_2^{\epsilon_k-1}\left(\lambda-\frac{1}{\Omega_1^{2\kappa(\lambda^{max})}\lambda^2}\right)\right\}, \tag{20}$$

where $\tilde{I}_1 = \Omega_1^{2\kappa(\lambda^{max})}\lambda^2+2\lambda^{-1}$ and $\tilde{I}_2 = 2\lambda+\Omega_1^{-2\kappa(\lambda^{max})}\lambda^{-2}$. The function $\kappa(\lambda^{max})$ is given by Eq. $(19)_3$ as: $\kappa(\lambda^{max}) = m_7\exp\left[m_8\,(\lambda^{max})^{m_9}\right]$. Parameter Ω_1 is obtained from Eq. (9) as:

$$\Omega_1 = \frac{b(\lambda^{max})+2}{b(\lambda^{max})+1}-\frac{1}{b(\lambda^{max})+\exp\left\{-c(\lambda^{max})\left[\lambda^{max}-\lambda\right]\left[\lambda^{max}-1\right]\right\}}, \tag{21}$$

where, from Eqs. $(19)_1$ and $(19)_2$, $b(\lambda^{max}) = m_1\exp\left[m_2\,(\lambda^{max})^{m_3}\right]$ and $c(\lambda^{max}) = m_4\exp\left[m_5\,(\lambda^{max})^{m_6}\right]$. The discontinuous inelasticity parameter Ω is then calculated from Eq. (8) on using the above Ω_1 and $\Omega_2 = \Omega_3 = 1$.

We start by correlating the model in Eq. (20) with the loading–unloading data of the epoxy specimens due to Uchida et al. (2022). The loading phase of this data was modelled in Section 3.2, and the obtained values for the *core* hyperinelastic model parameters were given in Table 2. By keeping those parameters fixed, Eq. (20) is fitted to the unloading phase of the dataset. Note that the dataset therein only includes one unloading cycle. As a result, functions $b(\bullet)$, $c(\bullet)$ and $\kappa(\bullet)$ reduce to single-valued parameters, since there is only one λ^{max} value involved here. We designate those single values here as b_0, c_0 and κ_0, for brevity. The modelling results are shown in Fig. 7, and Table 6 contains the identified values. The tabulated numerical datapoints of the unloading path have been given by Table A.2 of Appendix. The model is seen to capture the unloading behaviour successfully, with R^2 in excess of 0.97.

Table 6
The additional model paramter values of the augmented hyperinelastic function for capturing the unloading behaviour of the glassy polymer specimens reported in Uchida et al. (2022).

b_0 [–]	c_0 [–]	κ_0 [–]
0.26	61.70	-0.00_2

The next example we consider is the unloading behaviour of the high density polyethylene samples of Ayoub et al. (2010), the primary loading behaviour of which was considered in Section 3.3. Here the cyclic unloading behaviour of those specimens are considered, by simultaneously fitting the model in Eq. (20) to all five unloading cycles of that dataset. The numerical values of the collated datapoints have been listed in Table A.5 of Appendix. Note that the identified model parameter values of the *core* hyperinelastic function in modelling the loading phase, as given in Table 3, were again kept fixed, and only the m_z parameters were required to be optimised. The obtained fits are shown in the plots of Fig. 8(a), and the corresponding values of m_z are given in Table 7. The model is seen to capture this cyclic unloading behaviour reasonably well, with R^2 values in excess of 0.90.

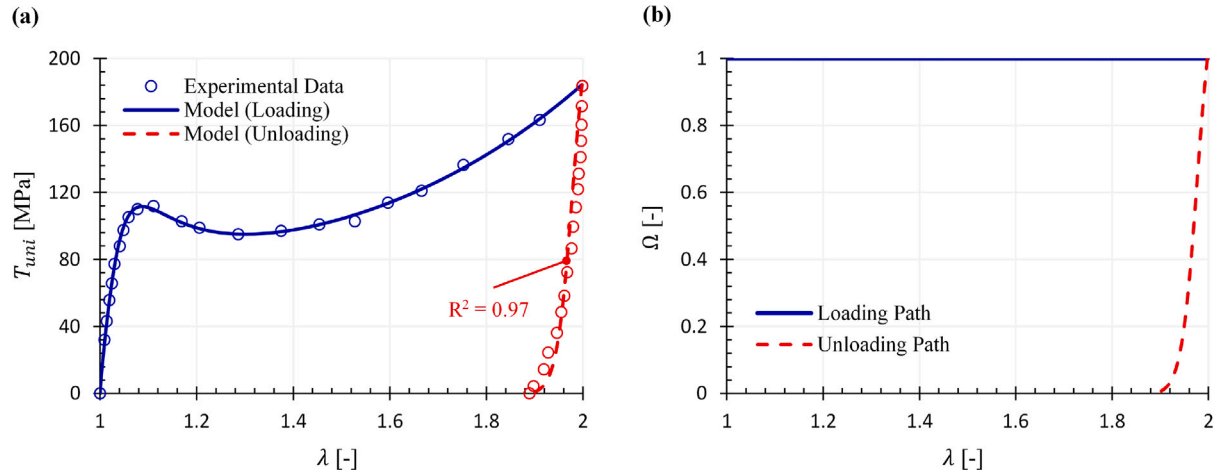

Fig. 7. Modelling the unloading behaviour of the epoxy polymer specimens reported in Uchida et al. (2022): (a) fitting with the data; and (b) the evolution of the inelasticity variable Ω with the deformation. The identified model parameter values of the *core* hyperinelastic function are those of Table 2, resulting from modelling the loading path, and were kept fixed here for modelling the unloading behaviour. The evolution of Ω at each λ has been calculated via Eq. (8), on using Eq. (21) to compute Ω_1 and $\Omega_2 = \Omega_3 = 1$.

Table 7
The obtained values of m_z, $(z = 1, \ldots, 9)$, for modelling the inelastic unloading behaviour of the semi-crystalline polymer specimens due to Ayoub et al. (2010).

m_1 [–]	m_2 [–]	m_3 [–]	m_4 [–]	m_5 [–]	m_6 [–]	m_7 [–]	m_8 [–]	m_9 [–]
0.26	−0.12	-7.18_5	30.67	4.10	-3.86_5	−0.10	−6.24	0.36

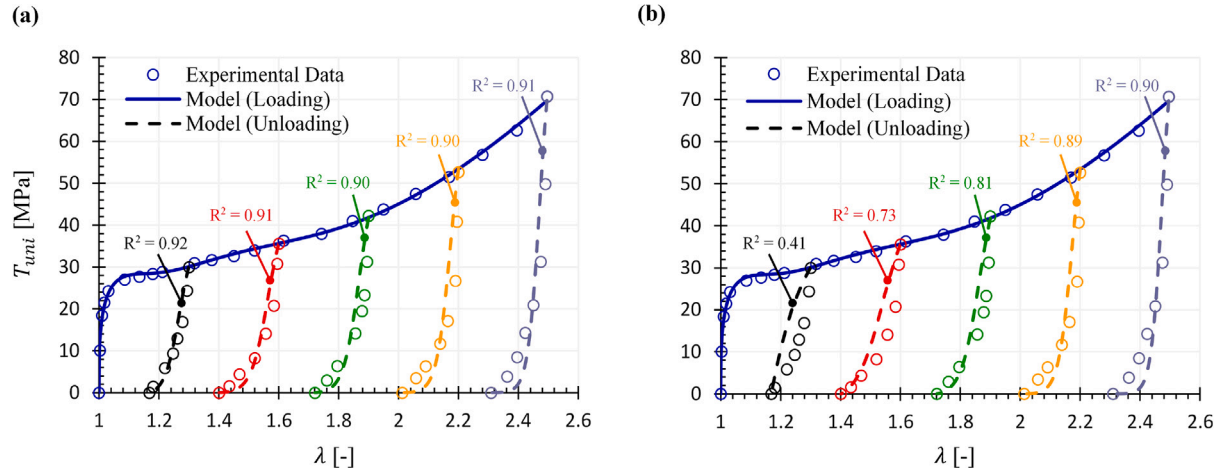

Fig. 8. Modelling the unloading behaviour of the semi-crystalline high density polyethylene specimens due to Ayoub et al. (2010): (a) on using the discontinuous inelasticity variable Ω_1 in Eq. (21); i.e., considering $b\left(\lambda_j^{max}\right)$, $c\left(\lambda_j^{max}\right)$ and $\kappa\left(\lambda_j^{max}\right)$; and (b) on using the discontinuous inelasticity variable Ω_1 in Eq. (22); i.e., considering b, c and κ as constant parameters. The identified model parameter values of the *core* hyperinelastic function are those of Table 3, resulting from modelling the loading path, and were kept fixed here when modelling the unloading behaviour. Values of the parameters m_z, $z = 1, \ldots, 9$, obtained for the fits in panel (a) have been given in Table 7. The ensuing values for b, c and κ of the fits in panel (b) are: $b = 0.26$ [–], $c = 37.27$ [–], and $\kappa = -0.00_{03}$ [–].

It may be worth noting that it is possible to treat $b(\bullet)$, $c(\bullet)$ and $\kappa(\bullet)$ as constant valued parameter (i.e., whose values remain the same across all unloading cycles). Doing so will considerably reduce the number of unloading parameters, effectively eliminating m_z, and the directional discontinuous inelasticity parameter Ω_1 in Eq. (21) simply becomes:

$$\Omega_1 = \frac{b+2}{b+1} - \frac{1}{b + \exp\left\{-c\left[\lambda^{max} - \lambda\right]\left[\lambda^{max} - 1\right]\right\}}, \tag{22}$$

where b and c are now mere constants. In the same way, Eq. (11) also simplifies to $\Gamma_j = \Omega_j^{\kappa}\,\lambda_j$. While this assumption may still qualitatively capture the unloading behaviour, the quality of the fits in the unloading paths reduce compared with the form in Eq. (21). For the interested reader, re-fitting of the model to this data on using constant b, c and κ; i.e., Eq. (22), has been presented in Fig. 8(b).

Vernerey et al. (2018) also provide the unloading behaviour for their quadruple-network hydrogel specimens, which we will consider here as another example for the application of the proposed augmented hyperinelastic model of this study. Similar to the previous exercise, the five unloading cycles were simultaneously fitted to the model in Eq. (20). Note that the primary loading path was already modelled using the *core* hyperinelastic function in Section 3.4, and the parameter values were identified and presented in Table 4. Those parameter values were kept fixed in modelling the unloading behaviour. In addition, since the unloading of these specimens did not leave a permanent set, $\kappa\left(\lambda_j^{max}\right) = 0$ due to Remark 5, and thus parameters m_7, m_8 and m_9 do not enter the model. There remain, therefore, only six additional parameters m_z, $z = 1,\ldots,6$, for capturing this unloading behaviour. The results are shown in the plots of Fig. 9, and the obtained values for the m_z parameters are given in Table 8. The model is seen to favourably capture the unloading behaviour of these samples, with R^2 values in excess of 0.97. The numerical datapoints for the unloading datasets have been tabulated and provided in Appendix, Table A.6.

Similar to Section 3, the final exemplar dataset considered here is for a LCE specimen subjected to a loading–unloading cycle under uniaxial deformation, due to Merkel et al. (2019). The inclusion of this dataset here is purely from the perspective of showcasing the capability of the proposed augmented hyperinelastic function in Eq. (15) to a wide range of elastomeric soft solids. For this dataset, since the original data has been provided in engineering stress, the one-term expansion of the model in Eq. (20) was first converted into $P_{uni} - \lambda$ form, where P denotes the engineering stress.[7] The ensuing $P_{uni} - \lambda$ relationship was then simultaneously fitted to both the loading and unloading data. Note that in the loading path, as explained in Remark 3, $\Omega_j = 1$ and $\Omega = 1$; therefore, Eq. (20) coincides with Eq. (7). In addition, since this dataset only includes one unloading cycle, functions $b(\bullet)$, $c(\bullet)$ and $\kappa(\bullet)$ reduce to single-valued parameters, as there is only one λ^{max} value involved. To be consistent with the results for Uchida et al. (2022) presented earlier in this section, we denote those single valued parameters here by b_0, c_0 and κ_0, respectively. The modelling results are shown in Fig. 10, and Table 9 contains the obtained model parameter values. The tabulated numerical datapoints for this dataset have been presented in Anssari-Benam et al. (2024).

Table 8
The identified values of m_z, $(z = 1,\ldots,6)$, for modelling the unloading behaviour of the quadruple-network hydrogel specimens due to Vernerey et al. (2018).

m_1 [–]	m_2 [–]	m_3 [–]	m_4 [–]	m_5 [–]	m_6 [–]
0.29	0.36	−1.96	0.00_8	8.76	−0.34

Table 9
Model parameter values for the loading–unloading behaviour of nematic-genesis polydomain LCE samples due to Merkel et al. (2019).

μ [kPa]	N [–]	n [–]	β [–]	C [kPa]	ϵ [–]	b_0 [–]	c_0 [–]	κ_0 [–]
31.99	0.98	0.95	1.86	311.51	0.50	0.03	1.57	0.00_1

The results indicate that the model captures the loading–unloading behaviour of this specimen favourably, with R^2 values in excess of 0.99. However, it is instructive to emphasise that capturing this behaviour for LCE specimens is not a trivial modelling task. As a case in point, Mihai and Goriely (2020) deemed it necessary to use a four-term expansion of the seminal Ogden model, within the framework of the 'neo-classical' theory for liquid crystal elastomers, to capture such loading–unloading behaviours, leading to a model with a rather elaborate form and 10 model parameters. The simple modelling approach presented here appears to provide an improvement to their modelling results.

I should like to close this section by highlighting a limitation of the proposed approach to modelling the unloading behaviour. The directional inelasticity variable Ω_j as defined by Eq. (9) returns the value $\Omega_j = 1$ in principal directions under compression, as explained by Remark 2. Consider a simple uniaxial compressive deformation in, say, direction '1'; i.e., $\lambda_1 = \lambda$ and $\lambda_2 = \lambda_3 = \lambda^{-0.5}$. Since in compression $\lambda_1 < 1$, we have $\Omega_1 = 1$, and in view of Eq. (11), no permanent set in the unloading path along direction '1' can be predicted or modelled. There are, however, various ways by which such nuanced features may be addressed. For example, Ω_j in Eq. (11) may be replaced by the discontinuous inelasticity parameter Ω of Eq. (8), and $b(\bullet)$, $c(\bullet)$ and $\kappa(\bullet)$ may be considered as functions of the final value of the stretch λ_j reached prior to the initiation of unloading in each unloading cycle, rather than the currently prescribed maximum value of the principal stretches in the history of loading before the initiation of unloading λ_j^{max}. My intention here, and throughout this work, has been to lay out the foundations of the proposed *hyperinelasticity* framework and modelling approach. The flexibility and versatility provided by this framework allows for further future improvements to the modelling details, as may be required.

[7] Note that $\mathbf{T} = \mathbf{F}\mathbf{P}$.

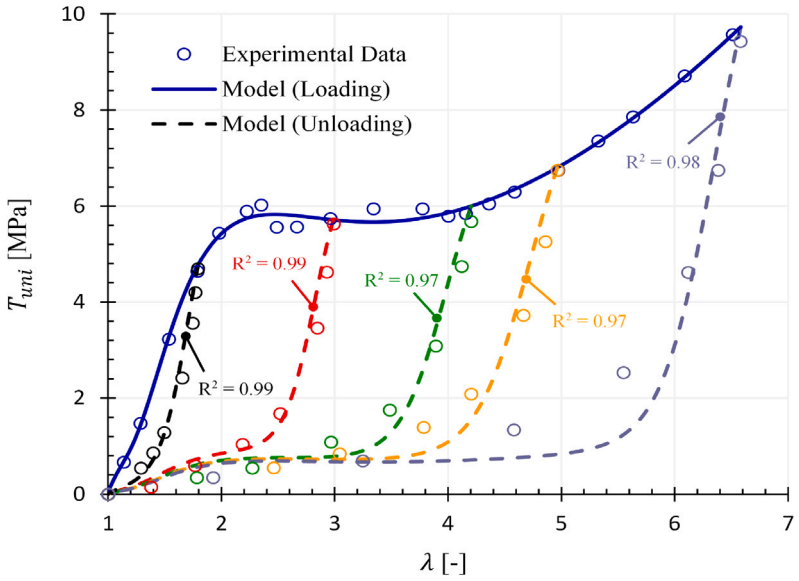

Fig. 9. Modelling the unloading behaviour of the quadruple-network hydrogel specimens of Vernerey et al. (2018). The identified model parameter values of the *core* hyperinelastic function are those of Table 4, resulting from modelling the loading path, and were kept fixed here when modelling the unloading behaviour.

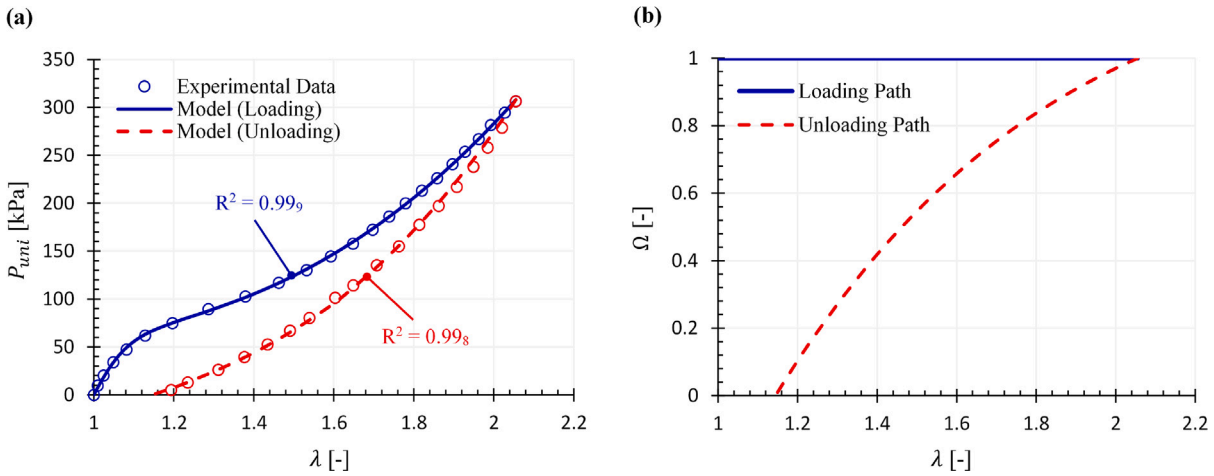

Fig. 10. Modelling results for the uniaxial loading–unloading of a nematic-genesis polydomain LCE sample due to Merkel et al. (2019): (a) fitting with the data; and (b) the evolution of the inelasticity variable Ω with the deformation. Note that the stress data is provided in engineering stress **P**. The (one-term expansion of the) model in Eq. (20), converted into $P_{uni} - \lambda$, was fitted simultaneously to the loading and unloading data. The evolution of Ω at each λ has been calculated via Eq. (8), on using Eq. (21) to compute Ω_1 and $\Omega_2 = \Omega_3 = 1$.

5. Incorporating the rate effects

Another manifestation of inelasticity in large deformation of polymers is the rate-dependency in the mechanical behaviour of the specimens. To cast a precise distinction between rate-dependency and other various time-dependent behaviours, we delineate this behaviour as follows: *rate-dependent* behaviour reflects itself in the instantaneous deformation response of the subject specimen to the applied deformation at various rates.

In modelling the *rate-dependent* behaviour so defined, it has been stipulated that the parameters of the *core* model may be considered to *evolve* with; i.e., be a function of, (a measure of) deformation rate (Anssari-Benam and Hossain, 2023). The application of this modelling framework within the bounds of hyperelasticity has successfully been shown for a wide range of elastomers, from hydrogels to LCEs (Anssari-Benam and Hossain (2023; 2024); Anssari-Benam and Saccomandi, 2024b). Here, the same approach is adopted for incorporation into the proposed *core* hyperinelastic model, in order to capture the rate-dependency in the large elastic and inelastic behaviours of polymers. In the sequel I provide the mathematical basis and thermodynamics consistency of this

modelling approach, followed by its application to the rate-dependent behaviour of the same open- and closed-cell polyurethane and closed-cell polystyrene foam specimens of Lee et al. (2020), whose quasi-static behaviour was modelled in Section 3.1.

5.1. The framework for modelling rate-dependency

The underlying basis in this framework is that for modelling the rate-dependent behaviour, the model parameters of the *core* function W may be considered to vary, i.e., *evolve*, with (a measure of) rate of deformation. Let us denote the resulting function, whose model parameters now are function of rate, by W^r, where the superscript r now denotes the rate-dependent form of the model, and refer to this function as the augmented hyperinelastic function by rate,[8]

Since, in rate-dependent deformation experiments, the *control variable* is the rate of deformation $\dot{\lambda}_j$, which is set in experiments to a pre-defined value, it is intuitive to consider that the measure of rate of deformation to be defined from $\dot{\mathbf{F}}$. Following Anssari-Benam and Hossain (2023), one such measure, denoted by $\dot{\varepsilon}$, may be considered as follows.

The rate of deformation set in experiments pertains to the rate of the *applied* deformation. Accordingly, let vector $\mathbf{a}$ define the information regarding the (principal) directions of the *applied* loading as:

$$\mathbf{a}=\left[\delta_1,\delta_2,\delta_3\right]^{\mathrm{T}}\ ,\quad \delta_j=\begin{cases}1\,, & \text{if } j \text{ is the direction of applied loading}\,,\\ 0\,, & \text{otherwise}\,.\end{cases} \tag{23}$$

Let tensor $\mathbf{A}$ then be constructed from $\mathbf{a}$ via:

$$\mathbf{A}=\mathbf{a}\otimes\mathbf{a}\,, \tag{24}$$

where $\otimes$ denotes the dyadic operator. The measure of deformation rate $\dot{\varepsilon}$ is accordingly defined as:

$$\dot{\varepsilon}=\max\left\{\left|\mathbf{A}\,\dot{\mathbf{F}}\right|\right\}\,, \tag{25}$$

i.e., the maximum of the absolute values of the arrays in the matrix $\mathbf{A}\,\dot{\mathbf{F}}$, where $\dot{\mathbf{F}}$ is the time-derivative of the deformation gradient $\mathbf{F}$; i.e., $\dot{\mathbf{F}}=\mathrm{diag}\left(\dot{\lambda}_j\right)$, $j=1,2,3$. It is therefore observed that in essence, the measure of deformation $\dot{\varepsilon}$ defined by Eq. (25) is equivalent to the absolute value of either of the corresponding components of $\dot{\lambda}_j$, $j=1,2,3$, whichever has the maximum absolute value.

Next, the modelling framework that utilises this measure is considered as follows. We define a free energy function $\widetilde{W}^r$ as:

$$\widetilde{W}^r=W^r-w\left(\dot{\mathbf{F}}\right)\,, \tag{26}$$

where:

$$W^r\equiv W\left(\mathbf{F},\dot{\mathbf{F}}\right)\,, \tag{27}$$

is the augmented hyperinelastic function by rate. W^r is indeed the extension of the *core* hyperinelastic energy function W by incorporating the deformation rate into its model parameters (i.e., the *core* model parameters of W in Eq. (1) *evolve* with, or are a *function* of, a defined measure of deformation rate). Within the context of the current work, the dependence of W^r on $\mathbf{F}$ is understood via the principal invariants I_1 and I_2 of the Cauchy–Green deformation tensor(s). Function w is an auxiliary function, only a function of $\dot{\mathbf{F}}$, which implies that:

$$\frac{\partial w\left(\dot{\mathbf{F}}\right)}{\partial\mathbf{F}}=\mathbf{0}\,. \tag{28}$$

The dependence of both W^r and w on $\dot{\mathbf{F}}$ is considered via the defined measure of deformation rate in Eq. (25). The functional form of w need not be specified, since due to Eq. (28) it will not enter the stress–deformation relationships. Its existence, however, is merely important from the point of view of thermodynamical consistency, as will be shown in the next section, and we accordingly require that:

$$\frac{\partial w\left(\dot{\mathbf{F}}\right)}{\partial\dot{\mathbf{F}}}=\frac{\partial W\left(\mathbf{F},\dot{\mathbf{F}}\right)}{\partial\dot{\mathbf{F}}}\,. \tag{29}$$

The specialised functional form of W^r may therefore now be expressed as:

$$W^r\equiv W\left(\mathbf{F},\dot{\mathbf{F}}\right)=W\left(I_1,I_2,\dot{\varepsilon}\right)=\sum_{i=1}^{}\frac{3\left[\phi_i\left(\dot{\varepsilon}\right)-1\right]}{2\phi_i\left(\dot{\varepsilon}\right)}\Omega_i\left(\dot{\varepsilon}\right)\xi_i\left(\dot{\varepsilon}\right)\left\{\frac{1}{3\xi_i\left(\dot{\varepsilon}\right)\left[\phi_i\left(\dot{\varepsilon}\right)-1\right]}\left(I_1-3\right)^{\Gamma_i(\dot{\varepsilon})}-\ln\left[\frac{I_1-3\xi_i\left(\dot{\varepsilon}\right)}{3-3\xi_i\left(\dot{\varepsilon}\right)}\right]^{\Gamma_i(\dot{\varepsilon})}\right\} \tag{30}$$

$$+\sum_{k=1}^{}\rho_k\left(\dot{\varepsilon}\right)\left[\left(\frac{I_2}{3}\right)^{\eta_k(\dot{\varepsilon})}-1\right],$$

[8] Not to be confused with the augmented hyperinelastic function $\widetilde{W}$ of Section 4 which was augmented by discontinuous inelasticity variables Ω_j for capturing the unloading behaviour.

where:

$$\mu_i \equiv \Omega_i\,(\dot{\epsilon})\,, \quad N_i \equiv \xi_i\,(\dot{\epsilon})\,, \quad n_i \equiv \phi_i\,(\dot{\epsilon})\,, \quad \beta_i \equiv \Gamma_i\,(\dot{\epsilon})\,, \quad C_k \equiv \rho_k\,(\dot{\epsilon})\,, \quad \epsilon_k \equiv \eta_k\,(\dot{\epsilon})\,, \tag{31}$$

and Ω_i, ξ_i, ϕ_i, Γ_i, ρ_k and η_k are, as yet, unspecified scalar functions of $\dot{\epsilon}$, whose exact functional forms may be designated empirically. We will specify these functions in Section 5.3.

5.2. Thermodynamics consistency

Considering only the mechanical contributions (i.e., discounting the temperature and heat transfer effects etc.), the Clausius–Duhem inequality reads (Holzapfel, 2000):

$$\mathcal{D} := \frac{1}{2}\mathbf{S} : \dot{\mathbf{C}} - \dot{\mathcal{W}} \geq 0\,, \tag{32}$$

where $\mathcal{D}$ is the rate of dissipation per unit volume, $\mathcal{W}$ is the *free* energy, $\dot{\mathcal{W}}$ is its time derivative, $\mathbf{S}$ and $\dot{\mathbf{C}}$ are the 2nd Piola–Kirchhoff and the time-derivative of the right Cauchy–Green tensors, respectively, and the operator $(:)$ is 'double contraction'.

Within the context of the current work, it is clear from Eq. (26) that the free energy of concern is $\widetilde{W}^r$. The Clausius–Duhem inequality in Eq. (32) may now be re-written on using Eq. (26) as:

$$\mathcal{D} := \frac{1}{2}\mathbf{S} : \dot{\mathbf{C}} - \dot{\widetilde{W}}^r \geq 0 \implies \mathcal{D} := \frac{1}{2}\mathbf{S} : \dot{\mathbf{C}} - \left(\dot{W}^r - \dot{w}\right) \geq 0\,. \tag{33}$$

By using the chain rule we find:

$$\dot{W}^r = \frac{\mathrm{d}W^r}{\mathrm{d}t} = \frac{\partial W^r}{\partial \mathbf{C}} : \frac{\partial \mathbf{C}}{\partial t} + \frac{\partial W^r}{\partial \dot{\mathbf{F}}} : \frac{\partial \dot{\mathbf{F}}}{\partial t}\,, \tag{34}$$

and:

$$\dot{w} = \frac{\mathrm{d}w}{\mathrm{d}t} = \frac{\partial w}{\partial \dot{\mathbf{F}}} : \frac{\partial \dot{\mathbf{F}}}{\partial t} = \frac{\partial W}{\partial \dot{\mathbf{F}}} : \frac{\partial \dot{\mathbf{F}}}{\partial t}\,, \tag{35}$$

where here use has been made of Eq. (29). Substituting Eqs. (34) and (35) into (33), and bearing in mind Eq. (27), yields straightforwardly:

$$\mathcal{D} = \frac{1}{2}\mathbf{S} : \dot{\mathbf{C}} - \left(\frac{\partial W^r}{\partial \mathbf{C}} : \dot{\mathbf{C}}\right) \geq 0\,. \tag{36}$$

This inequality is *a priori* satisfied since, in view of the condition in Eq. (28), the 2nd Piola–Kirchhoff tensor $\mathbf{S}$ is derived from W^r by definition as:

$$\mathbf{S} = 2\,\frac{\partial W^r}{\partial \mathbf{C}}\,. \tag{37}$$

5.3. Application to rate-dependent data

Deriving explicit stress–deformation relationships from the augmented hyperinelastic function by rate, i.e., W^r of Eq. (30), is contingent upon specifying the functional form(s) of the dependency of Ω_i, ξ_i, ϕ_i, Γ_i, ρ_k and η_k on $\dot{\epsilon}$. This choice remains empirical; however, it might be prudent to opt for a functional form that results in the least added number of model parameters. The simplest functional form may therefore be of linear dependency:

$$\begin{aligned} &\Omega_i\,(\dot{\epsilon}) = \mu_i + g_{1,i}\,\dot{\epsilon}\,, \quad \xi_i\,(\dot{\epsilon}) = N_i + g_{2,i}\,\dot{\epsilon}\,, \quad \phi_i\,(\dot{\epsilon}) = n_i + g_{3,i}\,\dot{\epsilon}\,, \\ &\Gamma_i\,(\dot{\epsilon}) = \beta_i + g_{4,i}\,\dot{\epsilon}\,, \quad \rho_k\,(\dot{\epsilon}) = C_k + g_{5,k}\,\dot{\epsilon}\,, \quad \eta_k\,(\dot{\epsilon}) = \epsilon_k + g_{6,k}\,\dot{\epsilon}\,, \end{aligned} \tag{38}$$

where $g_{z,i}$, $g_{z,k} \in \mathbb{R}$, $z = 1, \ldots, 6$, are the rate parameters, $g_{1,i}$ and $g_{5,k}$ have units of [Pa s], and all other $g_{z,i}$, $g_{z,k}$ are dimensionless.

One may now proceed with deriving the required stress–stretch relationships for application to the experimental data. In light of Eqs. (26) and (28), we note that the representation formula for computing the Cauchy stress may now be re-written as:

$$\mathbf{T} = -p\,\mathbf{I} + 2W_1^r\,\mathbf{B} - 2W_2^r\,\mathbf{B}^{-1}\,, \tag{39}$$

where W^r is the augmented hyperinelastic function specified in Eq. (30), and subscripts '1' and '2' denote the partial derivatives of W^r with respect to the principal invariants I_1 and I_2, respectively. Depending on each boundary value problem, the representation formula in Eq. (39) may be specialised for the respective deformation. However, similar to the applications in Sections 3 and 4, the experimental tests employed in the literature to investigate the rate-dependent behaviour of polymers appear to largely focus on uniaxial deformation. In particular, the dataset of Lee et al. (2020), which we wish to consider here as an archetypical example,

Table 10
The established values of the rate parameters $g_{z,i}$ and $g_{z,k}$, $z = 1, \ldots, 6$, in fitting the two-term expansion of the model in Eq. (40) to the rate-dependent behaviour of the closed-cell polyurethane specimens due to Lee et al. (2020). See Table 1 for the values of the *core* model parameters.

$g_{1,1}$ [MPa s]	$g_{2,1}$ [–]	$g_{3,1}$ [–]	$g_{4,1}$ [–]	$g_{5,1}$ [MPa s]	$g_{6,1}$ [–]
−0.29	-0.00_1	−0.09	−0.01	−0.09	−0.19
$g_{1,2}$ [MPa s]	$g_{2,2}$ [–]	$g_{3,2}$ [–]	$g_{4,2}$ [–]	$g_{5,2}$ [MPa s]	$g_{6,2}$ [–]
0.32	-0.00_2	1.00	0.03	−0.95	0.02_5

Table 11
The obtained values of the rate parameters $g_{z,1}$, $z = 1, \ldots, 6$, when fitting the one-term expansion of the model in Eq. (40) to the rate-dependent behaviour of open-cell polyurethane samples from (Lee et al., 2020). See Table 1 for the values of the *core* model parameters.

$g_{1,1}$ [MPa s]	$g_{2,1}$ [–]	$g_{3,1}$ [–]	$g_{4,1}$ [–]	$g_{5,1}$ [MPa s]	$g_{6,1}$ [–]
-0.83_5	−0.03	−5.01	0.00_5	−0.17	0.06

utilises uniaxial compression. Accordingly, here it suffices to only present the ensuing $T_{uni} - \lambda$ relationship. On noting that $\lambda_1 = \lambda$, $\lambda_2 = \lambda_3 = \lambda^{-0.5}$, $\dot{\epsilon} = \dot{\lambda}$, and subject to the assumption of plane stress $(T_{33} = 0)$, we find:

$$T_{uni} = \sum_{i=1} \frac{\Omega_i(\dot{\lambda})\,\Gamma_i(\dot{\lambda})}{\phi_i(\dot{\lambda})} \times \frac{I_1\left(I_1-3\right)^{\Gamma_i(\dot{\lambda})-1} + 3\xi_i(\dot{\lambda})\left[1-\left(I_1-3\right)^{\Gamma_i(\dot{\lambda})-1}\right] - 3\,\phi_i(\dot{\lambda})\,\xi_i(\dot{\lambda})}{I_1 - 3\,\xi_i(\dot{\lambda})} \times \left(\lambda^2 - \frac{1}{\lambda}\right) + \sum_{k=1} \frac{2\,\rho_k(\dot{\lambda})\,\eta_k(\dot{\lambda})}{3^{\eta_k(\dot{\lambda})}} I_2^{\eta_k(\dot{\lambda})-1} \left(\lambda - \frac{1}{\lambda^2}\right), \tag{40}$$

where $\Omega_i(\dot{\epsilon})$, $\xi_i(\dot{\epsilon})$, $\phi_i(\dot{\epsilon})$, $\Gamma_i(\dot{\epsilon})$, $\rho_k(\dot{\epsilon})$ and $\eta_k(\dot{\epsilon})$ are given in Eq. (38).

Using the same fitting method described in Section 3, the relationship in Eq. (40) will now be used for fitting with the experimental data of Lee et al. (2020). The first rate-dependent dataset we present here pertains to the closed-cell polyurethane specimens therein. In addition to the quasi-static deformation, which was considered in Section 3.1, Lee et al. (2020) also report stress–deformation curves at various rates. Here we consider the reported behaviours at $\dot{\lambda} = 0.075\ s^{-1}$, $0.7\ s^{-1}$ and $8.3\ s^{-1}$; i.e., over more than 100-fold range of deformation rate. This relatively wide range provides a robust initial test for examining the capability of the model in capturing the rate-dependent behaviour of polymers under large elastic and inelastic deformations. Accordingly, using the same *core* model parameter values given in Table 1, the three rate-dependent datasets were simultaneously fitted to the model in Eq. (40). Note that the two-term expansion of the model was used to fit with the quasi-static data in Section 3.1. The modelling results are given in the plots of Fig. 11, and the identified model parameter values are listed in Table 10. The numerical datapoints for the three rate-dependent datasets have been provided in Appendix, Table A.7. Given the complex behaviour of these specimens under compression, and the fact that only 12 model parameters were used in the fitting process (i.e., the 12 rate-dependent parameters $g_{z,i}$ and $g_{z,k}$ in Eq. (38), since the *core* model parameter values had been already established in Section 3.1 by fitting the *core* model to the quasi-static data), the model appears proficient in capturing the rate-dependent behaviour of these specimens.

The next example is regarding the rate-dependent behaviour of the open-cell polyurethane specimens from Lee et al. (2020). The quasi-static large elastic and inelastic behaviour of these samples was considered in Section 3.1, and the obtained *core* model parameter values were presented in Table 1. Here, we consider the reported datasets of their rate-dependent behaviour, tested under uniaxial compression at $\dot{\lambda} = 0.08\ s^{-1}$ and $4.6\ s^{-1}$. Recall that for the quasi-static dataset, the one-term form of the *core* model was sufficient. Accordingly, the one-term expansion of the rate model in Eq. (40) is simultaneously fitted here to the two rate-dependent datasets, with the *core* model parameter values being fixed (as given by Table 1). The modelling results are shown in Fig. 12, and the identified values of the six rate parameters $g_{z,1}$, $z = 1, \ldots, 6$, have been summarised in Table 11. The model is again seen to have captured the rate-dependent behaviour of these specimens favourably. The numerical datapoints for the two rate-dependent datasets have been tabulated and presented in Appendix, Table A.8.

The final example we consider here is the rate-dependent behaviour of the closed-cell polystyrene samples of Lee et al. (2020). For modelling the quasi-static behaviour of these specimens, the two-term expansion of the model was considered in Section 3.1, and the *core* hyperinelastic model parameter values were identified — see Table 1. Using those *core* model parameter values, the two-term expansion of the model in Eq. (40) was simultaneously fitted with the two reported rate-dependent datasets therein, tested at $\dot{\lambda} = 0.08\ s^{-1}$ and $4.6\ s^{-1}$, under uniaxial compression. The fitting results are illustrated in Fig. 13. The model is seen to have simulated the rate-dependent data most favourably, with R^2 values in excess of 0.99. The identified rate parameter values, $g_{z,i}$ and $g_{z,k}$ with $z = 1, \ldots, 6$, are contained in Table 12. See Table A.9 in Appendix for the tabulated numerical datapoints.

It may be worth noting that while the linear assumption for the functional dependency of the *core* model parameters on the (measure of) rate of deformation was sufficient here to capture the rate-dependent behaviour of the considered samples successfully,

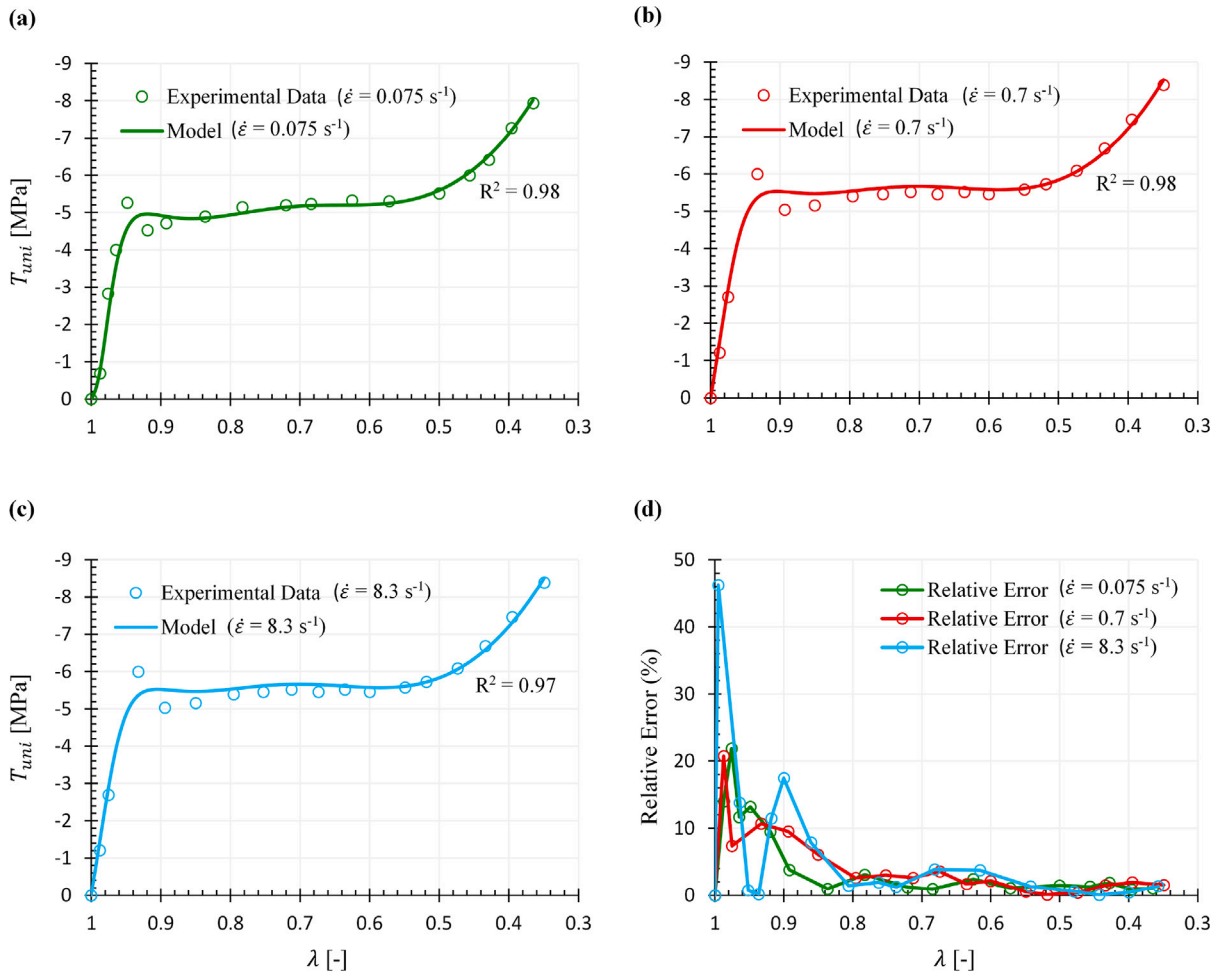

Fig. 11. Modelling results for the rate-dependent behaviour of closed-cell polyurethane foam samples due to Lee et al. (2020) under uniaxial compression at various deformation rates: (a) $\dot{\varepsilon} = 0.075$ s^{-1}; (b) $\dot{\varepsilon} = 0.75$ s^{-1}; (c) $\dot{\varepsilon} = 8.3$ s^{-1}; and (d) the ensuing relative errors. See the online version for plots in colour.

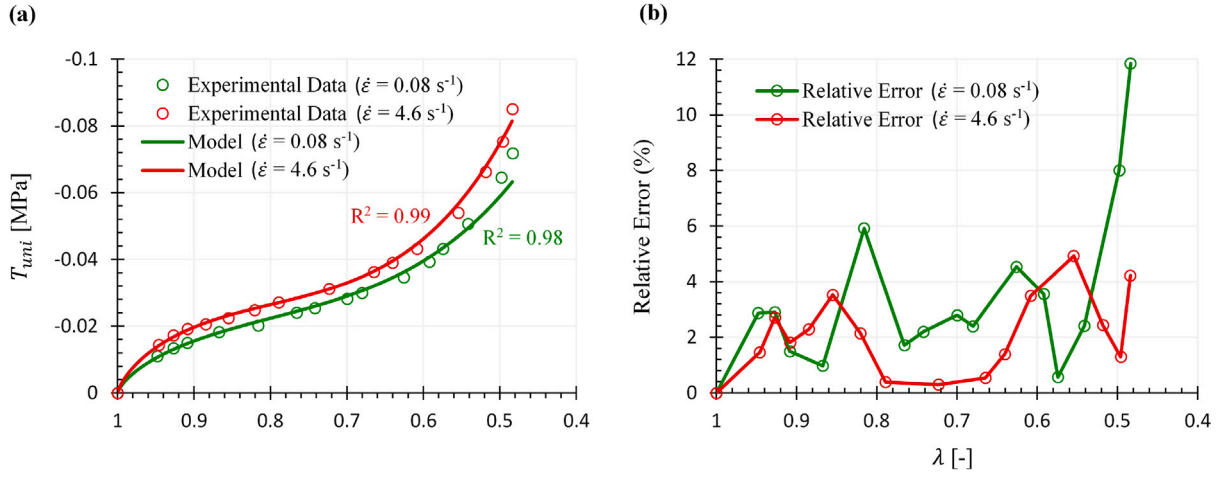

Fig. 12. Modelling results for the rate-dependent behaviour of open-cell polyurethane specimens from Lee et al. (2020) under uniaxial compression at two deformation rates, using the one-term expansion of the model in Eq. (40): (a) fitting with the data; and (b) the resulting relative error plots. See the online version for plots in colour.

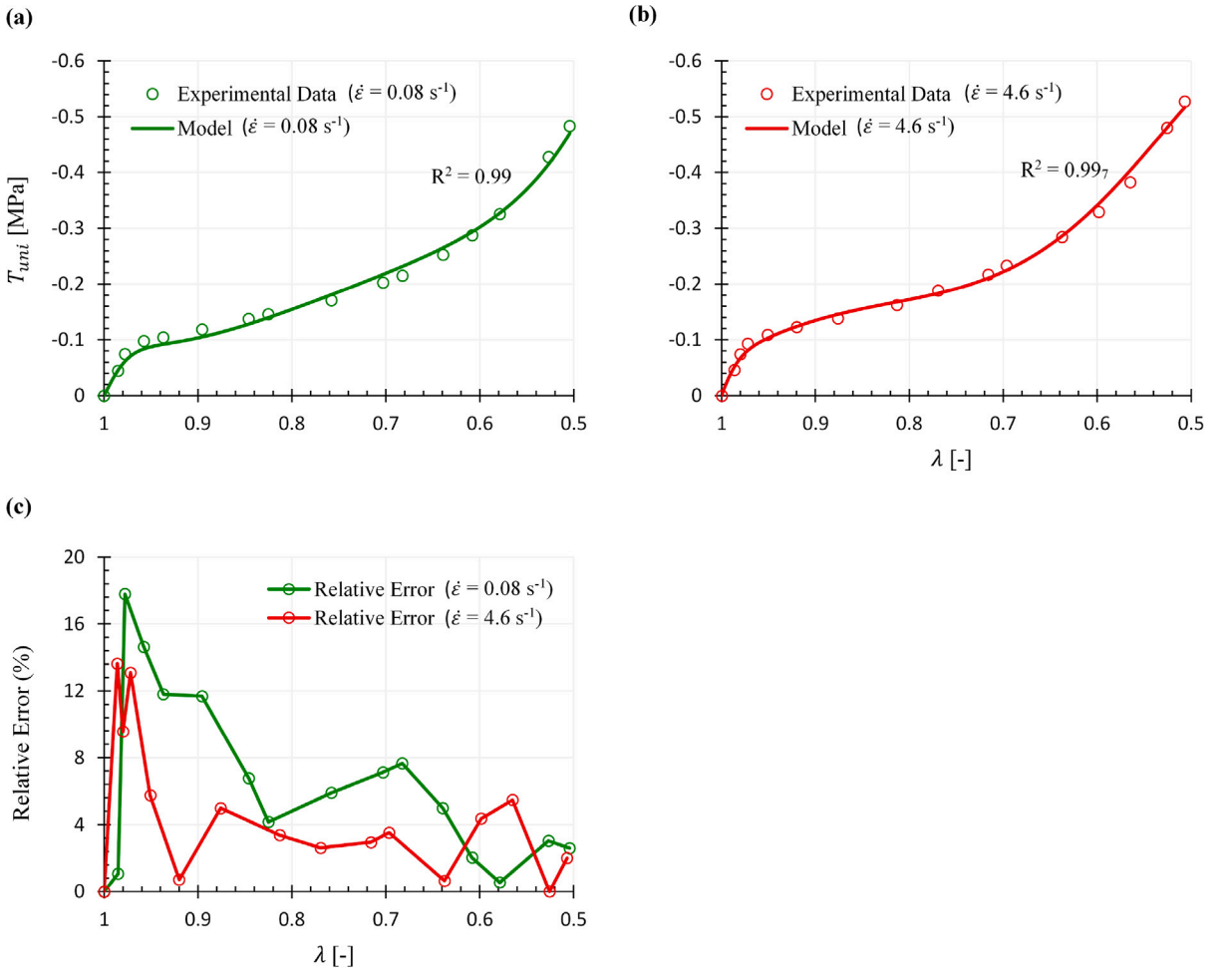

Fig. 13. Modelling results for the rate-dependent behaviour of closed-cell polystyrene foam specimens from Lee et al. (2020) under uniaxial compression at two deformation rates: (a) $\dot{\epsilon} = 0.08$ s^{-1}; (b) $\dot{\epsilon} = 4.6$ s^{-1}; and (c) the resulting relative error plots. See the online version for plots in colour.

Table 12
The identified values of the rate parameters $g_{z,i}$ and $g_{z,k}$, $z = 1, \ldots, 6$, in fitting the two-term expansion of the model in Eq. (40) to the rate-dependent behaviour of the closed-cell polystyrene foam specimens due to Lee et al. (2020). See Table 1 for the values of the *core* model parameters.

$g_{1,1}$ [MPa s]	$g_{2,1}$ [–]	$g_{3,1}$ [–]	$g_{4,1}$ [–]	$g_{5,1}$ [MPa s]	$g_{6,1}$ [–]
0.14	−0.67	−0.38	0.03	0.62	−0.01
$g_{1,2}$ [MPa s]	$g_{2,2}$ [–]	$g_{3,2}$ [–]	$g_{4,2}$ [–]	$g_{5,2}$ [MPa s]	$g_{6,2}$ [–]
−0.08	0.00_{02}	0.00_{5}	0.23	0.15	−0.07

more complex rate-dependent behaviours may necessitate the consideration of more elaborate dependencies. For example, in a recent study by Anssari-Benam and Saccomandi (2024b), for capturing the changes that incur in the soft elasticity plateau of LCE specimens under various rates, a three-parameter skewed exponential function of deformation rate was deemed more proficient, as was for capturing the rate-dependent softening of the brain tissue (Anssari-Benam and Saccomandi, 2024a). The same consideration may also be applied when the span of the deformation rate is wider than that considered here. For example, if one uses the identified rate parameters in Table 10 to predict the behaviour across one decade higher of deformation rate, i.e., over 1000-fold and above, the linear functional dependency assumption runs into difficulties to provide a reasonable estimation. The flexibility of the presented framework here accommodates for incorporation of more intricate rate-dependency functional assumptions, as may be required per different

applications. The consideration of more complex rate-dependent functions may particularly be prudent when the one-term form of the *core* hyperinelastic model is used, to help contain the total number of parameters in a given boundary value optimisation problem.

I should also note that the considered examples here, as per the original experimental studies, only focused on the rate-dependent behaviour of the specimens in the primary loading path. It is possible to extend the presented modelling formulations here to include the unloading behaviour as well, by simply considering that the discontinuous inelasticity variables Ω_j of Section 4.1 evolve with the rate of deformation as well. However, most datasets that I have come across thus far, from the unloading behaviour of hydrogels at various rates due to Mao et al. (2017) (see, e.g., Fig. 11 therein) to polymethyl methacrylate (PMMA) specimens of Uchida et al. (2022) (see, e.g., Figure 18 therein), indicate that the unloading path is *rate-insensitive*. That is, if the specimens are deformed up to the same λ^{max} at various rates, their unloading paths (and permanent sets) coincide; except for the initial starting point of stress which will naturally be different at different rates. However, this difference will already be captured by the model in the loading path. Therefore, it appears sufficient to only add the discontinuous inelasticity parameters into the augmented hyperinelastic model by rate, W^r, without the need to consider the discontinuous inelasticity parameters to evolve with rate. This postulate may be worth investigating in a separate undertaking.

6. Concluding remarks

This work aimed at laying the foundation for the concept of *hyperinelasticity*, for application to the large elastic and inelastic behaviours of polymers. Irrespective of the terminology, my intention was to present this concept by postulating that a single deformation energy W, of an appropriate choice, may be used for capturing and modelling the elastic and inelastic behaviours of the subject soft specimens. The inelastic behaviour of interest is the natural progression to the elastic phase, with the increase in the level of deformation. The constitutive parameters of the *hyperinelastic* deformation energy function W, if comprehensive enough, will then determine and capture both the elastic and inelastic behaviours, without the need for the usual added premises of yield/flow switches or damage parameters etc. Such an approach significantly simplifies the modelling endeavours of the inelastic behaviour of polymers, and in particular helps reducing the number of model parameters that need to be known/identified. The application of this concept, and a specific W function, to the deformation of a wide range of polymeric and elastomer specimens was demonstrated, ranging from foams, glassy and semi-crystalline polymers to hydrogels and liquid crystal elastomers. Encouraging initial results were observed and presented, indicative of the universal, versatile and accurate potential for the applicability of this concept, and model, to capturing the inelasticity of soft materials.

The presented *core* hyperinelastic model, as per the counterpart in hyperelasticity, is applicable to the (primary) loading path, for capturing the elastic phase followed by the peak (yield) stress, the softening and/or plateauing phase, and the eventual hardening regime before total failure. This *core* hyperinelastic function, then, may be specialised to incorporate additional inelastic behaviour features including the unloading behaviour and rate-dependency etc. The former was done by considering and devising a discontinuous inelasticity variable Ω, which is inactive in the primary loading path and takes effect only in the unloading phase. The latter was exemplified by allowing the *core* model parameters to vary with the deformation rate. The ensuing *augmented* hyperinelastic functions, $\widetilde{W}$ and W^r, respectively, were then applied to extant datasets of various samples, again demonstrating encouraging results in capturing such complex behaviours.

The presented theoretical framework, and the experimental datasets considered here, pertained to isothermal deformations only. This was done to simplify the first presentation of the devised approach, since the main intention in this manuscript was to provide the first theoretical basis for this modelling concept. The effects of temperature can, of course, be then incorporated into the *core* hyperinelastic function in various ways, one of which perhaps in a similar manner as the deformation rate was incorporated. That is, by allowing the *core* model parameters to evolve with temperature, subject to appropriate axioms and conditions to ensure that the Clausius–Duhem inequality is not violated. Incorporating the temperature effects may prove another versatile venue for the specialisation and application of the presented modelling approach here. In the absence of the temperature effects, however, the presented framework should provide a robust basis for capturing and modelling other inelastic behaviours, particularly in the loading path.

Depending on the perceived usefulness of the presented *hyperinelasticity* modelling framework for capturing the inelastic behaviour of polymers, and how well it may be received by the community, many further developments and specialisations may be made and incorporated into the basic model presented here. These may include more elaborate discontinuous functions to capture the unloading behaviour with better precision, more comprehensive rate-evolution functions that facilitate the capturing of the rate-effects over a wider span of deformation rates and allow predictability of the behaviour at other rates, improved *core* function(s) to more accurately model the primary loading path, and as discussed in the foregoing, incorporation of the temperature effects. These traits were not pursued here, as the objective in this work was to present the basic idea and provide the theoretical foundations.

On that note, given the success of the application of this framework to a wide range of polymers, capturing the complex elastic and inelastic behaviours in the loading path, favourable modelling of the discontinuous inelasticity in the unloading path, and encouraging results for the incorporation of the rate effects, this modelling approach, and the proposed *hyperinelastic* function, are presented as a versatile tool for modelling the macro-level elastic and inelastic behaviour of polymers. The reduced number of model parameters compared with the other existing models in the literature, and the innate simplicity of the implementation of the model (as essentially a straightforward extension to hyperelasticity), present themselves as notable advantages. Alternatively, given the success of the *core* hyperinelastic deformation energy function W utilised in this work on its own in capturing the elastic and inelastic behaviour in the loading path, the W function may be considered as a standard choice in other modelling frameworks which combine an elastic model with rheological features to simulate the inelastic behaviours of interest.

CRediT authorship contribution statement

Afshin Anssari-Benam: Writing – review & editing, Writing – original draft, Software, Methodology, Formal analysis, Data curation, Conceptualization.

Declaration of competing interest

I have no competing interests to declare.

Data availability

The numerical values of the experimental datapoints used in this work are tabulated and provided in Appendix of the manuscript, Tables A.1 to A.9.

Acknowledgements

I am grateful to Professor Fahmi Zaïri, University of Lille, for his insightful comments on an earlier draft of this manuscript.

Appendix. Tabulated numerical datapoints of the datasets used in this work

See Tables A.1–A.9.

Table A.1
Numerical datapoints from (Lee et al., 2020) for the uniaxial compression of their open- and closed-cell polyurethane, and closed-cell polystyrene, foam specimens.

Closed-cell polyurethane		Closed-cell polystyrene		Open-cell polyurethane	
λ [–]	T_{uni} [MPa]	λ [–]	T_{uni} [MPa]	λ [–]	T_{uni} [MPa]
1	0	1	0	1	0
0.98	-0.78_5	0.98	−0.05	0.95	-0.00_9
0.97	−2.15	0.96	−0.08	0.94	−0.01
0.95	−3.77	0.95	−0.09	0.92	-0.01_3
0.94_5	−4.81	0.93	−0.09	0.89	-0.01_4
0.93	−4.42	0.88	-0.10_6	0.87	-0.01_5
0.91	−4.23	0.84	-0.11_8	0.84	-0.01_6
0.89	−4.29	0.81	−0.12	0.81	-0.01_8
0.83	−4.55	0.77	−0.14	0.77	−0.02
0.77	−4.75	0.73_5	−0.15	0.71	-0.02_4
0.72	−4.88	0.70	−0.16	0.66	-0.02_7
0.66	−4.94	0.63	−0.20	0.61	−0.03
0.60	−4.77	0.57	-0.24_5	0.56	-0.03_7
0.56	−4.84	0.55	-0.26_5	0.54	−0.04
0.52	−5.03	0.53	−0.29	0.52	-0.04_4
0.48	−5.55	0.49	−0.35	0.48	−0.06
0.43_5	−6.13				
0.36	−7.48				

Table A.2
Numerical datapoints for the deformation of the poly(methyl methacrylate) epoxy specimens due to Ames et al. (2009), collated from (Uchida et al., 2022).

Loading path		Unloading path	
λ [–]	T_{uni} [MPa]	λ [–]	T_{uni} [MPa]
1	0	2.00	183.65
1.00_9	32.21	1.99_7	171.67
1.01_4	43.27	1.99_6	160.42
1.02	55.77	1.99_5	150.83
1.02_4	65.86_5	1.99_4	141.25
1.03	77.40	1.99	131.25
1.04	87.98	1.98_9	122.08
1.05	97.60	1.98_5	111.25
1.06	105.29	1.98	99.58
1.08	110.10	1.97_5	86.67
1.11	112.02	1.97	72.50
1.17	102.88_5	1.96	58.33
1.21	99.04	1.95_5	48.75
1.29	95.19	1.95	36.25
1.37	97.11_5	1.93	24.58
1.45	100.96	1.92	14.58
1.53	102.88_5	1.90	4.58
1.60	113.94	1.89	0
1.66_5	121.15		
1.75	136.54		
1.84_5	151.92		
1.91	163.46		
2.00	183.65		

Table A.3
Tabulated numerical datapoints for the uniaxial tension of high density polyethylene samples due to Ayoub et al. (2010). This table contains the data for the primary loading path only. See Table A.5 for the unloading data.

λ [–]	T_{uni} [MPa]
1	0
1.00_3	10.07
1.01	18.37
1.01_8	21.46
1.03	24.23
1.08_5	27.00
1.13	27.69
1.18	28.38_5
1.21	28.84_5
1.32	30.98
1.38	31.68
1.45	32.60
1.52	33.99
1.62	36.30
1.74	37.92
1.85	41.01
1.95	43.78
2.06	47.46_5
2.17	51.46
2.28	56.77
2.39_5	62.63
2.49_5	70.69

Table A.4
Datapoints collated from (Vernerey et al., 2018) on uniaxial tension of a quadruple-network hydrogel specimen. This table contains the data for the primary loading path only. See Table A.6 for the unloading data.

λ [–]	T_{uni} [MPa]
1	0
1.14	0.67
1.29	1.47_5
1.53	3.22
1.79	4.63_5
1.98	5.44
2.22	5.89
2.35	6.02_5
2.49	5.56
2.67	5.57
2.96	5.74
3.34	5.94_5
3.77	5.94_5
4.00	5.79
4.15_5	5.84
4.36	6.04_5
4.59	6.30
4.97	6.75
5.32_5	7.35_5
5.63	7.86
6.09	8.71_5
6.51	9.57

Table A.5
Tabulated numerical datapoints for the unloading cycles of the high density polyethylene samples due to Ayoub et al. (2010).

1st unloading cycle		2nd unloading cycle		3rd unloading cycle		4th unloading cycle		5th unloading cycle	
λ [–]	T_{uni} [MPa]	λ [–]	T_{uni} [MPa]	λ [–]	T_{uni} [MPa]	λ [–]	T_{uni} [MPa]	λ [–]	T_{uni} [MPa]
1.30	30	1.6 0	35.58	1.90	42.25	2.20	52.65	2.49_5	70.69
1.29	24.31	1.59	30.80	1.89_5	31.29	2.19_5	40.82	2.49	49.83
1.28	16.86	1.58	20.71	1.89	23.26_5	2.19	26.74	2.47	31.29
1.26	12.94	1.55_5	14.07	1.88	19.46	2.16	17.09	2.45	20.86
1.25	9.31	1.52	8.23	1.86	14.15	2.14	11.71	2.42	14.29
1.22	5.88	1.47	4.38	1.79_5	6.39	2.09	6.33	2.40	8.50
1.18	1.47	1.43_5	1.59	1.76	2.92_5	2.06	3.48	2.36	3.86
1.17	0	1.40	0	1.72	0	2.01	0	2.31	0

Table A.6
Tabulated numerical datapoints for the unloading cycles of the quadruple-network hydrogel specimens of Vernerey et al. (2018).

1st unloading cycle		2nd unloading cycle		3rd unloading cycle		4th unloading cycle		5th unloading cycle	
λ [–]	T_{uni} [MPa]	λ [–]	T_{uni} [MPa]	λ [–]	T_{uni} [MPa]	λ [–]	T_{uni} [MPa]	λ [–]	T_{uni} [MPa]
1.79_5	4.69	2.99	5.63	4.20	5.68	4.96	6.75	6.58	9.43
1.77	4.20	2.93	4.62	4.12	4.74	4.86	5.26	6.38	6.75
1.75	3.55_5	2.84	3.46	3.89	3.09	4.67	3.72	6.12	4.61_5
1.65	2.42	2.52	1.68	3.49	1.75	4.20	2.08	5.55	2.53
1.49	1.28	2.18_5	1.04	2.96	1.09	3.78	1.39	4.58	1.34
1.40	0.86	1.77	0.59	2.27	0.54	3.04	0.84	3.25	0.69_5
1.29	0.54	1.39	0.15	1.78	0.35	2.46	0.55	1.93	0.35
1	0	1	0	1	0	1	0	1	0

Table A.7
Numerical datapoints from (Lee et al., 2020) for the rate-dependent uniaxial compression of their closed-cell polyurethane foam specimens.

$\dot{\lambda} = 0.075\ s^{-1}$		$\dot{\lambda} = 0.7\ s^{-1}$		$\dot{\lambda} = 8.3\ s^{-1}$	
λ [–]	T_{uni} [MPa]	λ [–]	T_{uni} [MPa]	λ [–]	T_{uni} [MPa]
1	0	1	0	1	0
0.99	−0.69	0.99	−1.21	0.99_5	−0.56
0.98	−2.83	0.97_5	−2.70	0.96	-4.48_5
0.96_5	−4.00	0.93	−6.00	0.95	−6.00
0.948	−5.27	0.89	−5.04	0.94	−6.67
0.92	−4.53	0.85	−5.16	0.92	−6.09
0.89	-4.71_5	0.80	−5.40	0.90	−5.61
0.84	−4.90	0.75	−5.46	0.86	−5.61
0.78	−5.14	0.71	−5.52	0.81	−6.03
0.72	-5.20_5	0.67	−5.46	0.76	−6.03
0.68	−5.24	0.63_5	−5.52	0.74	−6.18
0.62_5	−5.33	0.60	−5.46	0.68	−6.09
0.57	−5.30	0.55	−5.58	0.61_5	−5.97
0.50	−5.51	0.52	−5.73	0.54	−6.33
0.46	−6.00	0.47	−6.09	0.48	−6.75
0.43	−6.41	0.43	−6.69	0.44	−7.34
0.40	−7.27	0.39_5	−7.46	0.40	−8.17
0.36_5	−7.94	0.35	−8.39	0.36	−9.16

Table A.8
Tabulated datapoints from (Lee et al., 2020) for the rate-dependent uniaxial compression of open-cell polyurethane foam samples.

$\dot{\lambda} = 0.08\ s^{-1}$		$\dot{\lambda} = 4.6\ s^{-1}$	
λ [–]	T_{uni} [MPa]	λ [–]	T_{uni} [MPa]
1	0	1	0
0.95	−0.01	0.95	−0.01
0.93	-0.01_3	0.93	-0.01_7
0.91	-0.01_5	0.91	-0.01_9
0.87	-0.01_8	0.88_5	−0.02
0.82	−0.02	0.85_5	-0.02_2
0.77	-0.02_4	0.82	-0.02_5
0.74	-0.02_5	0.79	-0.02_7
0.70	−0.03	0.72	−0.03
0.68	−0.03	0.66_5	-0.03_6
0.63	-0.03_5	0.64	-0.03_9
0.59	−0.04	0.61	−0.04
0.57	-0.04_3	0.55	−0.05
0.54	−0.05	0.52	-0.06_6
0.50	-0.06_5	0.50	-0.07_5
0.48	−0.07	0.48	-0.08_5

Table A.9
Numerical datapoints from (Lee et al., 2020) for the rate-dependent uniaxial compression of the closed-cell polystyrene foam specimens.

$\dot{\lambda} = 0.08\ s^{-1}$		$\dot{\lambda} = 4.6\ s^{-1}$	
λ [–]	T_{uni} [MPa]	λ [–]	T_{uni} [MPa]
1	0	1	0
0.98_5	-0.04_5	0.99	−0.05
0.98	-0.07_5	0.98	−0.07
0.96	−0.10	0.97	−0.09
0.94	-0.10_4	0.95	−0.11
0.90	−0.12	0.92	−0.12
0.84_5	−0.14	0.88	−0.14
0.82_5	−0.15	0.81	−0.16
0.76	−0.17	0.77	−0.19
0.70	−0.20	0.71_5	−0.22
0.68	-0.21_5	0.70	−0.23
0.64	−0.25	0.64	−0.28
0.61	−0.29	0.60	−0.33
0.58	-0.32_5	0.56_5	−0.38
0.53	−0.43	0.52_5	−0.48
0.50	−0.48	0.51	−0.53

References

Ahzi, S., Makradi, A., Gregory, R.V., Edie, D., 2003. Modeling of deformation behavior and strain-induced crystallization in poly(ethylene terephthalate) above the glass transition temperature. Mech. Mater. 35, 1139–1148. http://dx.doi.org/10.1016/S0167-6636(03)00004-8.

Akbari, R., Morovati, V., Dargazany, R., 2022. Reverse physically motivated frameworks for investigation of strain energy function in rubber-like elasticity. Int. J. Mech. Sci. 221, 107110. http://dx.doi.org/10.1016/j.ijmecsci.2022.107110.

Ames, N.M., Srivastava, V., Chester, S.A., Anand, L., 2009. A thermo-mechanically coupled theory for large deformations of amorphous polymers. Part II: Applications. Int. J. Plast. 25, 1495–1539. http://dx.doi.org/10.1016/j.ijplas.2008.11.005.

Anand, L., Ames, N.M., 2006. On modeling the micro-indentation response of an amorphous polymer. Int. J. Plast. 22, 1123–1170. http://dx.doi.org/10.1016/j.ijplas.2005.07.006.

Anand, L., Ames, N.M., Srivastava, V., Chester, S.A., 2009. A thermo-mechanically coupled theory for large deformations of amorphous polymers. Part I: Formulation. Int. J. Plast. 25, 1474–1494. http://dx.doi.org/10.1016/j.ijplas.2008.11.004.

Anssari-Benam, A., 2023. Continuous softening up to the onset of failure: A hyperelastic modelling approach with *intrinsic* softening for isotropic incompressible soft solids. Mech. Res. Commun. 132, 104183. http://dx.doi.org/10.1016/j.mechrescom.2023.104183.

Anssari-Benam, A., 2024. A generalised $W\left(I_1, I_2\right)$ strain energy function of binomial form with unified applicability across various isotropic incompressible soft solids. Acta Mech. 235, 99–132. http://dx.doi.org/10.1007/s00707-023-03677-1.

Anssari-Benam, A., Akbari, R., Dargazany, R., 2023. Extending the theory of pseudo-elasticity to capture the permanent set and the induced anisotropy in the Mullins effect. Int. J. Non-Linear Mech. 156, 104500. http://dx.doi.org/10.1016/j.ijnonlinmec.2023.104500.

Anssari-Benam, A., Hossain, M., 2023. A pseudo-hyperelastic model incorporating the rate effects for isotropic rubber-like materials. J. Mech. Phys. Solids 179, 105347. http://dx.doi.org/10.1016/j.jmps.2023.105347.

Anssari-Benam, A., Hossain, M., 2024. A unified pseudo-elastic model of *continuous* and *discontinuous* softening in the finite deformation of isotropic soft solids. Int. J. Solids Struct. 290, 112670. http://dx.doi.org/10.1016/j.ijsolstr.2024.112670.

Anssari-Benam, A., Saccomandi, G., 2024a. Continuous softening as a state of hyperelasticity: Examples of application to the softening behavior of the brain tissue. J. Biomech. Eng. 146, 091009. http://dx.doi.org/10.1115/1.4065271.

Anssari-Benam, A., Saccomandi, G., 2024b. A model for capturing the *rate-dependent* mechanical behaviour of liquid crystal elastomers. Mech. Mater. submitted for publication.

Anssari-Benam, A., Wei, Z., Bai, R., 2024. Modelling the deformation of polydomain liquid crystal elastomers as a state of hyperelasticity. J. Elasticity http://dx.doi.org/10.1007/s10659-024-10055-y.

Arruda, E.M., Boyce, M.C., 1993. A three-dimensional constitutive model for the large stretch behavior of rubber elastic materials. J. Mech. Phys. Solids 41, 389–412. http://dx.doi.org/10.1016/0022-5096(93)90013-6.

Ayoub, G., Zaïri, F., Fréderix, C., Gloaguen, J.M., Naït-Abdelaziz, M., Seguela, R., Lefebvre, J.M., 2011. Effects of crystal content on the mechanical behaviour of polyethylene under finite strains: Experiments and constitutive modelling. Int. J. Plast. 27, 492–511. http://dx.doi.org/10.1016/j.ijplas.2010.07.005.

Ayoub, G., Zaïri, F., Naït-Abdelaziz, M., Gloaguen, J., 2010. Modelling large deformation behaviour under loading–unloading of semicrystalline polymers: Application to a high density polyethylene. Int. J. Plast. 26, 329–347. http://dx.doi.org/10.1016/j.ijplas.2009.07.005.

Beatty, M.F., 1987. Topics in finite elasticity: Hyperelasticity of rubber, elastomers, and biological tissues—with examples. Appl. Mech. Rev. 40, 1699–1734. http://dx.doi.org/10.1115/1.3149545.

Boyce, M.C., Parks, D.M., Argon, A.S., 1988. Large inelastic deformation of glassy polymers. part I: rate dependent constitutive model. Mech. Mater. 7, 15–33. http://dx.doi.org/10.1016/0167-6636(88)90003-8.

Carroll, M.M., 2011. A strain energy function for vulcanized rubbers. J. Elasticity 103, 173–187. http://dx.doi.org/10.1007/s10659-010-9279-0.

Cherief, M.N.D., Zaïri, F., Ding, N., Gloaguen, J.M., Naït-Abdelaziz, M., Benguediab, M., 2020. Plasticity and thermally-induced recovery in polycarbonate. Mech. Mater. 148, 103515. http://dx.doi.org/10.1016/j.mechmat.2020.103515.

van Dommelen, J.A.W., Parks, D.M., Boyce, M.C., Brekelmans, W.A.M., Baaijens, F.P.T., 2003. Micromechanical modeling of the elasto-viscoplastic behavior of semi-crystalline polymers. J. Mech. Phys. Solids 51, 519–541. http://dx.doi.org/10.1016/S0022-5096(02)00063-7.

Ehret, A.E., Itskov, M., 2009. Modeling of anisotropic softening phenomena: Application to soft biological tissues. Int. J. Plast. 25, 901–919. http://dx.doi.org/10.1016/j.ijplas.2008.06.001.

Gent, A.N., 1996. A new constitutive relation for rubber. Rubber Chem. Technol. 69, 59–61. http://dx.doi.org/10.5254/1.3538357.

Haward, R.N., Thackray, G., 1968. The use of a mathematical model to describe isothermal stress-strain curves in glassy thermoplastics. Proc. R. Soc. Lond. Ser. A Math. Phys. Eng. Sci. 302, 453–472. http://dx.doi.org/10.1098/rspa.1968.0029.

Holzapfel, G.A., 2000. Nonlinear Solid Mechanics: A Continuum Approach for Engineering. John Wiley and Sons Ltd, Chichester, England, pp. 161–176.

Khan, A.S., Suh, Y.S., Kazmi, R., 2004. Quasi-static and dynamic loading responses and constitutive modeling of titanium alloys. Int. J. Plast. 20, 2233–2248. http://dx.doi.org/10.1016/j.ijplas.2003.06.005.

Khiêm, V.N., Itskov, M., 2017. An averaging based tube model for deformation induced anisotropic stress softening of filled elastomers. Int. J. Plast. 90, 96–115. http://dx.doi.org/10.1016/j.ijplas.2016.12.007.

Lee, V., Bhattacharya, K., 2023. Universal deformations of incompressible nonlinear elasticity as applied to ideal liquid crystal elastomers. J. Elasticity http://dx.doi.org/10.1007/s10659-023-10018-9.

Lee, J.H., Ryu, D.-M., Lee, C.S., 2020. Constitutive-damage modeling and computational implementation for simulation of elasto-viscoplastic-damage behavior of polymeric foams over a wide range of strain rates and temperatures. Int. J. Plast. 130, 102712. http://dx.doi.org/10.1016/j.ijplas.2020.102712.

Lee, V., Wihardja, A., Bhattacharya, K., 2023. A macroscopic constitutive relation for isotropic-genesis, polydomain liquid crystal elastomers. J. Mech. Phys. Solids 179, 105369. http://dx.doi.org/10.1016/j.jmps.2023.105369.

Mao, Y., Lin, S., Zhao, X., Anand, L., 2017. A large deformation viscoelastic model for double-network hydrogels. J. Mech. Phys. Solids 100, 103–130. http://dx.doi.org/10.1016/j.jmps.2016.12.011.

Martin Linares, C.P., Traugutt, N.A., Saed, M.O., Martin Linares, A., Yakacki, C.M., 2020. The effect of alignment on the rate-dependent behavior of a main-chain liquid crystal elastomer. Soft Matter 16, 8782–8798. http://dx.doi.org/10.1039/D0SM00125B.

Merkel, D.R., Shaha, R.K., Yakacki, C.M., Frick, C.P., 2019. Mechanical energy dissipation in polydomain nematic liquid crystal elastomers in response to oscillating loading. Polymer 166, 148–154. http://dx.doi.org/10.1016/j.polymer.2019.01.042.

Mihai, L.A., Goriely, A., 2011. Positive or negative poynting effect? The role of adscititious inequalities in hyperelastic materials. Proc. R. Soc. A. 467, 3633–3646. http://dx.doi.org/10.1098/rspa.2011.0281.

Mihai, L.A., Goriely, A., 2020. A pseudo-anelastic model for stress softening in liquid crystal elastomers. Proc. R. Soc. A. 476, 20200558. http://dx.doi.org/10.1098/rspa.2020.0558.

Morovati, V., Bahrololoumi, A., Dargazany, R., 2021. Fatigue-induced stress-softening in cross-linked multi-network elastomers: Effect of damage accumulation. Int. J. Plast. 142, 102993. http://dx.doi.org/10.1016/j.ijplas.2021.102993.

Ogden, R.W., Roxburgh, D.G., 1999. A pseudo–elastic model for the Mullins effect in filled rubber. Proc. R. Soc. Lond. A. 455, 2861–2877. http://dx.doi.org/10.1098/rspa.1999.0431.

Ogden, R.W., Saccomandi, G., Sgura, I., 2004. Fitting hyperelastic models to experimental data. Comput. Mech. 34, 484–502. http://dx.doi.org/10.1007/s00466-004-0593-y.

Rezaei, L., Scalet, G., Peigney, M., Azoug, A., 2024. Coupling between viscoelasticity and soft elasticity in main-chain nematic Liquid Crystal Elastomers. J. Mech. Phys. Solids 187, 105612. http://dx.doi.org/10.1016/j.jmps.2024.105612.

Rivlin, R.S., 1948. Large elastic deformations of isotropic materials IV. further developments of the general theory. Philos. Trans. R. Soc. Lond. Ser. A 241, 379–397. http://dx.doi.org/10.1098/rsta.1948.0024.

Tokumoto, H., Zhou, H., Takebe, A., Kamitani, K., Kojio, K., Takahara, A., Bhattacharya, K., Urayama, K., 2021. Probing the in-plane liquid-like behavior of liquid crystal elastomers. Sci. Adv. 7, eabe9495. http://dx.doi.org/10.1126/sciadv.abe9495.

Treloar, L.R.G., 1943. The elasticity of a network of long-chain molecules - II. Trans. Faraday Soc. 39, 241–246. http://dx.doi.org/10.1039/TF9433900241.

Tvergaard, V., 1981. Influence of voids on shear band instabilities under plane strain conditions. Int. J. Fract. 17, 389–407. http://dx.doi.org/10.1007/BF00036191.

Uchida, M., Kamimura, K., Yoshida, T., Kaneko, Y., 2022. Viscoelastic-viscoplastic modeling of epoxy based on transient network theory. Int. J. Plast. 153, 103262. http://dx.doi.org/10.1016/j.ijplas.2022.103262.

Vernerey, F.J., Brighenti, R., Long, R., Shen, T., 2018. Statistical damage mechanics of polymer networks. Macromolecules 51, 6609–6622. http://dx.doi.org/10.1021/acs.macromol.8b01052.

Xiao, R., Mai, T.T., Urayama, K., Gong, J.P., Qu, S., 2021. Micromechanical modeling of the multi-axial deformation behavior in double network hydrogels. Int. J. Plast. 137, 102901. http://dx.doi.org/10.1016/j.ijplas.2020.102901.

Yan, Z., Guo, Q., Zaïri, F., Zaoui, A., Jiang, Q., Liu, X., 2021. Continuum-based modeling large-strain plastic deformation of semi-crystalline polyethylene systems: Implication of texturing and amorphicity. Mech. Mater. 162, 104060. http://dx.doi.org/10.1016/j.mechmat.2021.104060.

Yeoh, O.H., 1990. Characterisation of elastic properties of carbon-black-filled rubber vulcanizates. Rubber Chem. Technol. 63, 792–805. http://dx.doi.org/10.5254/1.3538289.

Zhan, L., Wang, S., Qu, S., Steinmann, P., Xiao, R., 2023. A new micro–macro transition for hyperelastic materials. J. Mech. Phys. Solids 171, 105156. http://dx.doi.org/10.1016/j.jmps.2022.105156.